

Supporting Information for

Ligand Field Effects on the Ground and Excited States of Reactive FeO²⁺ Species

Justin K. Kirkland¹, Shahriar N. Khan², Bryan Casale¹, Evangelos Miliordos^{2,*}, Konstantinos D. Vogiatzis^{1,*}

¹ Department of Chemistry, University of Tennessee, Knoxville, Tennessee 37996, United States

² Department of Chemistry and Biochemistry, Auburn University, Auburn, Alabama 36849, United States

Table of Contents

Section	Page
S1. Examination of Different Active Spaces	S-2
S2. Details on the Geometry Coordinates of the Fe(IV)-oxo Models	S-4
S3. Bare [FeO] ²⁺ Results from MRCI	S-10
S4. Analysis the of sigma/pi channels	S-16
S5. Active Space Molecular Orbitals from CASSCF Calculations	S-25
S6. Geometry Coordinates from Symmetric Ligand Scan Geometries	S-32

S1. Examination of Different Active Spaces

Structure	Active Space	Absolute CASSCF Energies (a.u.)	Dominant Configuration(s)	CI Coefficient
$[\text{Fe}(\text{O})(\text{H}_2\text{O})_5]^{2+}$	CAS(10,8)	-1726.41262059	222uuuu0 2u2duuuu	0.70275 0.10806
	CAS(10,13)	-1726.49941643	222uuuu0 00000 2u2duuuu 00000	0.73739 0.07872
	CAS(18,12)	-1726.43981644	2222222uuuu0 22222u2duuuu	0.70205 0.10400
	RAS(18,12)	-1726.43977403	2222222uuuu0 22222u2duuuu	0.70191 0.10390
$[\text{Fe}(\text{O})(\text{H}_2\text{O})_4]^{2+}$	CAS(10,8)	-1650.24633190	222uuuu0 u22duuuu	0.72081 0.09620
	RAS(22,14)	-1650.27544067	222222222uuuu0 222222u22duuuu	0.71252 0.09545
$[\text{Fe}(\text{O})(\text{H}_2\text{O})_{\text{ax}}(\text{NH}_3)_4]^{2+}$	CAS(10,8)	-1646.97217912	2u22uu0u ud22uuuu 0u22uu2u	0.80836 0.03308 0.04262
	RAS(24,15)	-1647.00507061	2222222 2u22uu0u 2222222 ud22uuuu 2222222 0u22uu2u	0.80551 0.03027 0.03783
	RAS(26,16)	-1647.00533346	22222222 2u22uu0u 22222222 ud22uuuu 22222222 0u22uu2u	0.80566 0.03020 0.03777
	RAS(28,17)	-1647.00543248	222222222 2u22uu0u 222222222 ud22uuuu 222222222 0u22uu2u	0.80564 0.03017 0.03771
	RAS(30,18)	-1647.00553460	2222222222 2u22uu0u 2222222222 ud22uuuu 2222222222 0u22uu2u	0.80561 0.03017 0.03767
	RAS(32,19)	-1647.00556318	22222222222 2u22uu0u 22222222222 ud22uuuu 22222222222 0u22uu2u	0.80555 0.03018 0.03768
$[\text{Fe}(\text{O})(\text{H}_2\text{O})_{\text{ax}}(\text{NH}_3)_3]^{2+}$	RAS(22,14)	-1590.72835843	222222 222uuuu0 222222 2u2duuuu	0.73057 0.06848
$[\text{Fe}(\text{O})(\text{NH}_3)_4]^{2+}$	RAS(24,15)	-1570.87276760	2222222 222uuuu0 2222222 22uduuuu	0.72358 0.06911
	RAS(28,17)	-1570.87375007	22222222 222uuuu0 22222222 22uduuuu	0.72358 0.06911

Table S1: Comparison of CASSCF/RASSCF energies, dominant electronic configurations and CI vectors.

Structure	Active Space	$E_{\text{gap}} (\sigma-\pi) \text{ at } R_{\text{Fe-O}}=1.6\text{\AA}$ (eV)
$[\text{Fe(O)(H}_2\text{O)}_5]^{2+}$	CAS(10,8)	1.23
	CAS(10,13)	1.13
	CAS(18,12)	1.24
	RAS(18,12)	1.24
$[\text{Fe(O)(H}_2\text{O)}_4]^{2+}$	CAS(10,8)	1.29
	CAS(20,13)	1.30
	RAS(22,14)	1.28
$[\text{Fe(O)(H}_2\text{O)}_{\text{ax}}(\text{NH}_3)_4]^{2+}$	CAS(18,12)	1.65
	RAS(22,14)	1.62
	RAS(24,15)	1.67
$[\text{Fe(O)(H}_2\text{O)}_{\text{ax}}(\text{NH}_3)_3]^{2+}$	CAS(20,13)	1.56
	RAS(22,14)	1.53
	RAS(24,15)	1.51
$[\text{Fe(O)(NH}_3)_4]^{2+}$	CAS(20,13)	1.79
	RAS(22,14)	1.77
	RAS(24,15)	1.77

Table S2: MS(3)-CASPT2 or MS(3)-RASPT2 energy differences between the ground quintet state and the first doubly degenerate quintet excited state at $R_{\text{Fe-O}} = 1.60 \text{ \AA}$ by considering different active space size. Results from a CAS(10,8) for the three models with strong ligand fields are not included, i.e. $[\text{Fe(O)(H}_2\text{O)}_{\text{ax}}(\text{NH}_3)_4]^{2+}$, $[\text{Fe(O)(H}_2\text{O)}_{\text{ax}}(\text{NH}_3)_3]^{2+}$ and $[\text{Fe(O)(NH}_3)_4]^{2+}$, since the lack of ligand orbitals introduced instabilities in the potential energy curves.

S2. Details on the Geometry Coordinates of the Fe(IV)-oxo Models

In two recent publications, Kazaryan and Baerends¹, and Andrikopoulos et al.² used the same model complexes ($[\text{Fe}(\text{O})(\text{H}_2\text{O})_5]^{2+}$, $[\text{Fe}(\text{O})(\text{NH}_3)_4(\text{H}_2\text{O})]^{2+}$) as in our work. A short comparison between their results obtained with the BLYP and OLYP density functionals, respectively, as well as with other popular functionals and multiconfigurational methods is presented in Table S3. All calculations were performed on the structures reported in Ref. 2.

For the ($[\text{Fe}(\text{O})(\text{H}_2\text{O})_5]^{2+}$) case, results from CASPT2 are in agreement with those from hybrid functionals (B3LYP and OLYP). On the contrary, for the strong field case ($[\text{Fe}(\text{O})(\text{NH}_3)_4(\text{H}_2\text{O})]^{2+}$), all single-point calculations with multiconfigurational methods predict the wrong ground spin state (quintet rather than the triplet). Addition of orbitals from the ligand field (lone pair of nitrogen atoms) reduced the energy gap between the two spin states from -19.7 (CASPT2(10,8)) to -5.5 kcal/mol (CASPT2(18,12)), but the triplet is still the ground state. The addition of the second shell (4d) orbitals and 3p orbitals of Fe didn't affect significantly the energy difference. As it has been discussed by others,³⁻⁴ disagreement between multireference and DFT results might occur in strong fields, which can be solved by optimization at the CASSCF or CASPT2 level. For that reason, we have calculated separately potential energy curves along the symmetrical dissociation of the Fe-NH₃ bonds. For sake of consistency, the same procedure was repeated for the $[\text{Fe}(\text{O})(\text{H}_2\text{O})_5]^{2+}$ model complex (symmetric dissociation of the Fe-H₂O bond distances). A CAS(10,8) active space that includes the five 3d orbitals of Fe and the three 2p orbitals of O is adequate for the two models with only H₂O ligands. Thus, the symmetric scans for the $[\text{Fe}(\text{O})(\text{H}_2\text{O})_4]^{2+}$ and $[\text{Fe}(\text{O})(\text{H}_2\text{O})_5]^{2+}$ models were performed at the MS-CASPT2(10,8) level. On the contrary, for obtaining the correct spin energy difference of the three models that include the strong donor NH₃ ligands, the addition of the 3s3p of Fe, the 2s of oxygen and ligand orbitals was mandatory. Those additions increase the size of the active space to (24,15) for the models. Since multi-state CASPT2 scans with many roots per spin state performed with these active spaces are computationally expensive, the MS-RASPT2 scheme was preferred. The additional lone pair orbitals of NH₃, the 3s3p of Fe and the 2s of the oxygen were included into the RAS1 space, while RAS2 included the important orbitals of the FeO²⁺ moiety. One- and two-electron excitations to RAS2 were allowed.

Level of Theory	Quintet – Triplet ΔE (kcal/mol)	
	$[\text{Fe}(\text{O})(\text{H}_2\text{O})_5]^{2+}$	$[\text{Fe}(\text{O})(\text{NH}_3)_4(\text{H}_2\text{O})]^{2+}$
TPSS	-6.7	16.9
BLYP	-5.8	17.4
BLYP ^a	-5.2	12.3
B3LYP	-16.4	6.8
OLYP ^b	-16.1	3.8
CASSCF(10,8)	-22.4	-24.1
CASPT2(10,8)	-22.8	-19.7
CASPT2(18,12)	-	-5.5
SA-RASSCF(24,15)	-	-15.2
MS-RASPT2(24,15)	-	-8.3
RASSCF(30,18)	-	-16.0
RASPT2(30,18)	-	-5.9

^a From Ref. 1.
^b From Ref. 2.

Table S3: Comparison between different levels of theory (DFT and multiconfigurational methods) for the two complexes under study.

1. $[\text{Fe}(\text{O})(\text{H}_2\text{O})_4]^{2+}$: CASPT2(10,8)

CAS: 3d of Fe, 2p of O

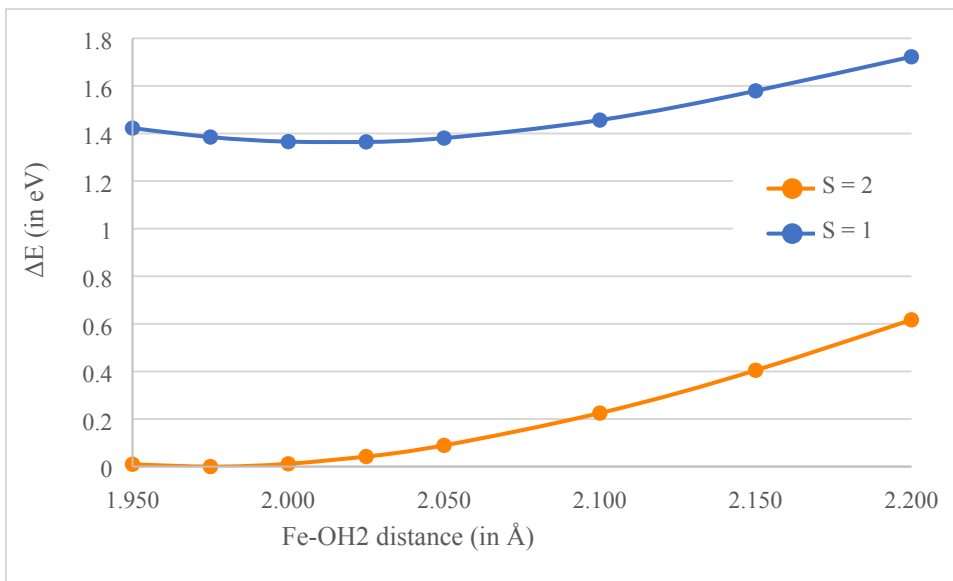


Figure S1: Potential energy curves for the symmetric dissociation of the three Fe-O bonds of $[\text{Fe}(\text{O})(\text{H}_2\text{O})_4]^{2+}$ (pseudo- C_{3v} symmetry).

For all Fe-OH₂ bond distances along equatorial plane the quintet state is the ground state with a minimum of 1.975 Å. This makes sense considering both the weak field nature of the water ligands as well the C_{3v} symmetry of the species.

2. $[\text{Fe}(\text{O})(\text{H}_2\text{O})_5]^{2+}$: CASPT2(10,8)

CAS: 3d of Fe, 2p of O

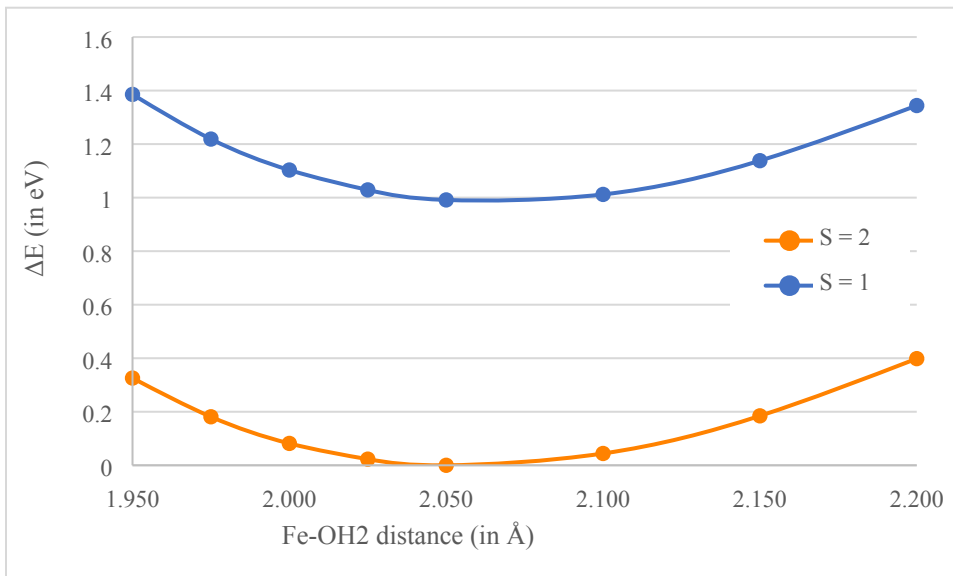


Figure S2: Potential energy curves for the symmetric dissociation of the three Fe-O bonds of $[\text{Fe}(\text{O})(\text{H}_2\text{O})_5]^{2+}$ (pseudo- C_{4v} symmetry).

Similarly, the weak field of the water ligands favors the quintet at all distances over the scan, with the minimum being at 2.050 Å.

3. $[\text{Fe}(\text{O})(\text{H}_2\text{O})_{\text{ax}}(\text{NH}_3)_3]^{2+}$: RASPT2(22,14)

RAS1: 3s3p of Fe, 2s of O, lone pair of NH₃

RAS2: 3d of Fe, 2p of O

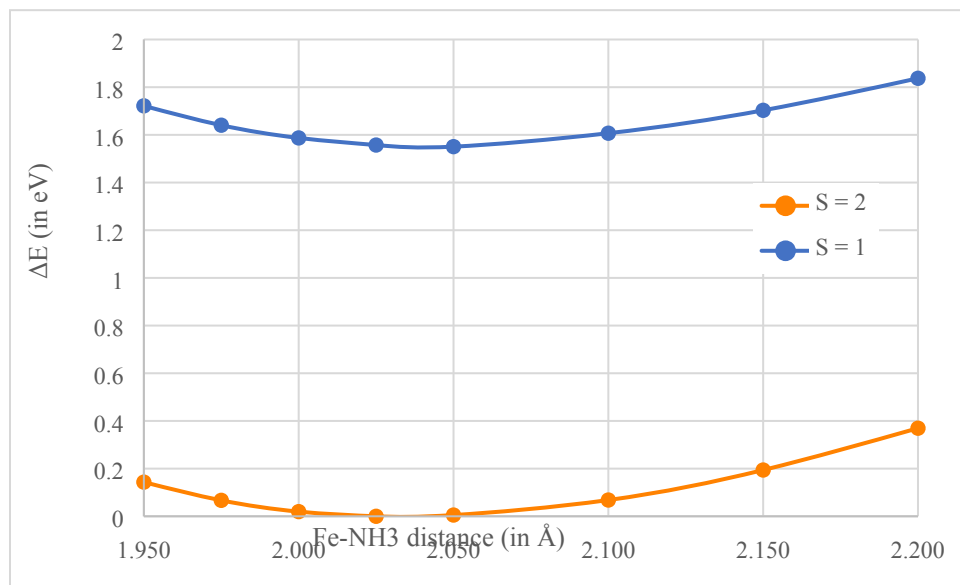


Figure S3: Potential energy curves for the symmetric dissociation of the three Fe-O bonds of $[\text{Fe}(\text{O})(\text{H}_2\text{O})_{\text{ax}}(\text{NH}_3)_3]^{2+}$ (pseudo- C_{3v} symmetry).

The quintet spin state is the ground state for $[\text{Fe}(\text{O})(\text{H}_2\text{O})_{\text{ax}}(\text{NH}_3)_3]^{2+}$, with the difference that this time a stronger field formed by ammonia ligands is applied. The pseudo- C_{3v} geometry stabilizes the quintet state over the triplet state, similarly to the $[\text{Fe}^{\text{IV}}(\text{O})(\text{TMG}_3\text{tren})]^{2+}$ species.⁵ This biomimetic molecular complex has its minimum at 2.050 Å for the Fe-N bond distances on the equatorial plane.

4. $[\text{Fe}(\text{O})(\text{H}_2\text{O})_{\text{ax}}(\text{NH}_3)_4]^{2+}$ ACTIVE SPACE: RASPT2(24,15)

RAS1: 3s3p of Fe, 2s of O, lone pairs of NH₃ (x2)

RAS2: 3d of Fe, 2p of O

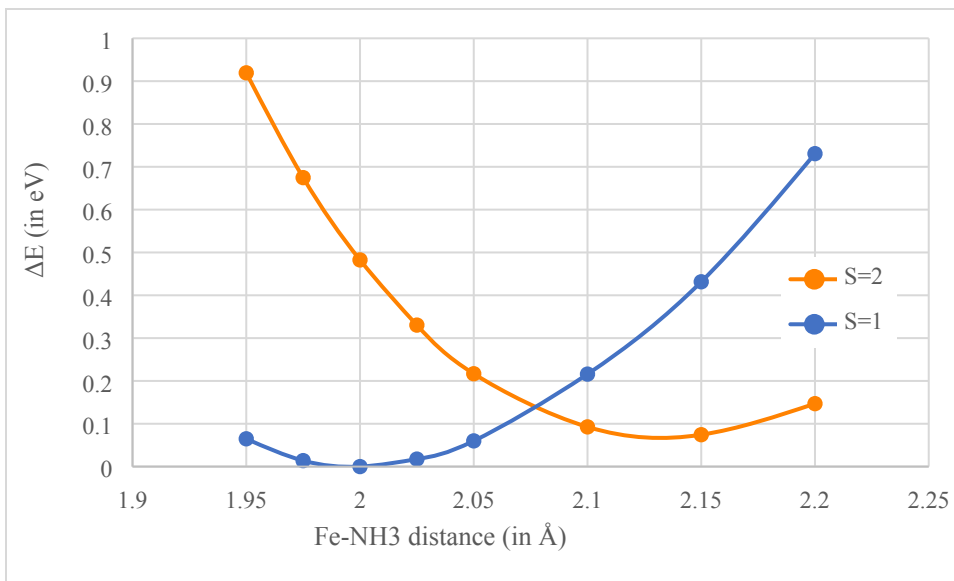


Figure S4: Potential energy curves for the symmetric dissociation of the three Fe-O bonds of $[\text{Fe}(\text{O})(\text{H}_2\text{O})_{\text{ax}}(\text{NH}_3)_4]^{2+}$ (pseudo- C_{4v} symmetry).

In the case of the pseudo- C_{4h} species, the triplet state is preferred with a ground state, with a Fe-NH₃ bond distance of 2.000 Å. For this system, the SA-RASSCF/MS-RASPT2 level was applied with 3 roots for the quintet and 6 roots for the triplet calculation, since those states are degenerate/dear-degenerate at the specific Fe-NH₃ bond range.

5. $[\text{Fe}(\text{O})(\text{NH}_3)_4]^{2+}$: RASPT2(24,15)

RAS1: 3s3p of Fe, 2s of O, lone pair of NH₃ (x2)

RAS2: 3d of Fe, 2p of O

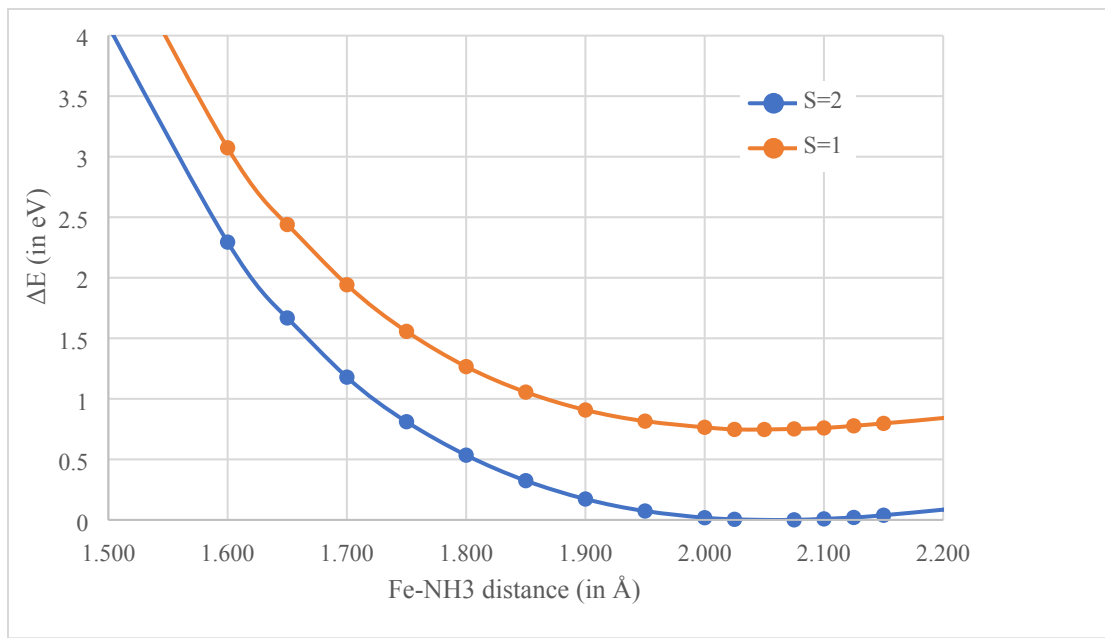


Figure S5: Potential energy curves for the symmetric dissociation of the three Fe-O bonds of $[\text{Fe}(\text{O})(\text{NH}_3)_4]^{2+}$ (pseudo- C_{3v} symmetry).

The pseudo- C_{3v} symmetry, despite the presence of strong field ligands, has a more stable quintet spin state than the triplet. In this case, the equilibrium Fe-N bond distance on the equatorial plane is 2.050 Å.

S3. Bare [FeO]²⁺ Results from MRCI

Spectroscopic constants, equilibrium bond lengths, and excitation energies of all twenty-seven states at the MRCI and MRIC+Q level are reported in Table S4, while their CI vectors are listed in Table S5. MOs that included in the active space for the MRCI calculations are shown in Figure S6.

State	Method	$-E_e$	r_e	ω_e	$\Delta G_{1/2}$	$\omega_e x_e$	α_e	T_e
$^3\Delta$	MRCI	1336.838198	2.108	344	339	2.4	0.0018	0
	MRCI+Q	1336.855001	2.101	343	339	2.4	0.0022	0
$^5\Delta$	MRCI	1336.837437	2.150	357	352	2.6	0.0021	167
	MRCI+Q	1336.853835	2.146	358	353	2.5	0.0029	256
$^7\Delta$	MRCI	1336.835622	2.197	368	362	3.1	0.0029	565
	MRCI+Q	1336.852080	2.194	370	364	3.2	0.0023	641
$^7\Pi$	MRCI	1336.834437	2.131	342	338	2.3	0.0034	826
	MRCI+Q	1336.851269	2.115	341	337	2.1	0.0016	819
$^5\Pi$	MRCI	1336.834246	2.140	334	328	3.2	0.0029	867
	MRCI+Q	1336.850951	2.129	334	325	3.9	0.0017	889
$^3\Pi$	MRCI	1336.834067	2.152	341	338	2.4	0.0036	907
	MRCI+Q	1336.850741	2.145	342	341	2.2	0.0021	935
$^3\Sigma^-$	MRCI	1336.826154	2.247	308	302	2.5	0.0026	2643
	MRCI+Q	1336.842858	2.236	311	305	2.4	0.0025	2665
$^5\Sigma^-$	MRCI	1336.824410	2.280	310	305	2.5	0.0025	3026
	MRCI+Q	1336.840671	2.270	313	308	2.4	0.0027	3145
$^7\Sigma^-$	MRCI	1336.822158	2.320	311	305	2.7	0.0028	3520
	MRCI+Q	1336.837489	2.312	314	309	2.6	0.0030	3843
$^5\Sigma^+$	MRCI	1336.810998	1.647	629	590	21.9	0.0147	5970
	MRCI+Q	1336.836551	1.634	701	653	21.7	0.0102	4049
$^3\Pi$	MRCI	1336.800547	1.855	282	252	1.5	0.0139	8263
	MRCI+Q	1336.816436	1.835	325	314	4.0	0.0180	8464
$^3\Phi$	MRCI	1336.800454	1.655	190	183	-3.1	0.0237	8284

	MRCI+Q	1336.816313	1.630	298	367	4.6	0.0345	8491
$^3\Sigma^+$	MRCI	1336.796459	2.036	278	308	4.7	-0.0015	9161
	MRCI+Q	1336.814915	2.026	303	340	6.8	-0.0027	8798
$^3\Delta$	MRCI	1336.796126	1.945	267	216	2.7	0.0098	9234
	MRCI+Q	1336.814626	1.924	292	251	4.3	0.0130	8861
$^5\Phi$	MRCI	1336.794840	2.122	267	258	3.9	0.0048	9516
	MRCI+Q	1336.813600	2.105	269	262	3.6	0.0055	9086
$^5\Pi$	MRCI	1336.794705	2.132	269	261	4.0	0.0047	9545
	MRCI+Q	1336.813368	2.118	273	265	3.9	0.0050	9137
$^3\Sigma^-$	MRCI	1336.793511	2.114	267	259	4.1	0.0049	9808
	MRCI+Q	1336.812455	2.100	269	261	3.9	0.0056	9338
$^7\Sigma^+$	MRCI	1336.793451	2.090	273	267	4.5	0.0034	9821
	MRCI+Q	1336.812353	2.058	269	284	2.8	0.0015	9360
$^5\Delta$	MRCI	1336.791094	2.208	258	248	4.6	0.0053	10338
	MRCI+Q	1336.810391	2.199	262	253	4.4	0.0051	9791
$^7\Pi$	MRCI	1336.790566	2.288	250	240	4.6	0.0053	10454
	MRCI+Q	1336.808828	2.281	254	245	4.5	0.0051	10134
$^5\Sigma^-$	MRCI	1336.790032	2.233	249	239	4.6	0.0058	10571
	MRCI+Q	1336.809134	2.226	252	243	4.4	0.0049	10067
$^7\Phi$	MRCI	1336.789723	2.282	251	241	4.6	0.0048	10639
	MRCI+Q	1336.808386	2.275	256	246	4.5	0.0049	10231
$^7\Pi$	MRCI	1336.788948	2.299	238	229	4.7	0.0061	10809
	MRCI+Q	1336.807631	2.287	244	235	4.7	0.0055	10396
$^5\Pi$	MRCI	1336.788165	2.242	192	186	2.5	0.0032	10981
	MRCI+Q	1336.807427	2.203	189	184	1.7	0.0035	10441
$^7\Delta$	MRCI	1336.787322	2.354	227	218	4.7	0.0051	11166
	MRCI+Q	1336.804966	2.351	230	221	4.6	0.0048	10981
$^7\Sigma^-$	MRCI	1336.786821	2.367	223	213	4.7	0.0053	11276
	MRCI+Q	1336.804146	2.365	225	216	4.6	0.0054	11161
$^3\Pi$	MRCI	1336.786701	2.316	198	190	3.8	0.0052	11302
	MRCI+Q	1336.805406	2.292	202	195	3.6	0.0043	10885

Table S4: Electronic energy E_e (a.u.), equilibrium bond lengths r_e (\AA), harmonic vibrational frequency ω_e (cm^{-1}), energy difference between the ground and first excited vibrational energy levels $\Delta G_{1/2}$ (cm^{-1}), anharmonicity $\omega_e x_e$ (cm^{-1}), rovibrational coupling constant α_e (cm^{-1}), and excitation energies T_e (cm^{-1}) for twenty seven electronic states of $^{56}\text{Fe}^{16}\text{O}^{2+}$.

State	Electronic configuration									
	1σ	2σ	3σ	4σ	1π _x	2π _x	1π _y	2π _y	1δ ₊	1δ ₋
³ Δ	0.38	2	2	α	0	β	α	β	α	α
	-0.34	2	2	α	0	β	α	2	0	α
	-0.34	2	2	α	0	2	0	β	α	α
⁵ Δ	0.56	2	2	α	0	β	α	α	α	α
	0.45	2	2	α	0	α	α	β	α	α
⁷ Δ	0.98	2	2	α	0	α	α	α	α	α
⁷ Π	0.96	2	2	α	0	α	α	α	2	α
⁵ Π	0.52	2	2	α	0	β	α	α	2	α
	0.48	2	2	α	0	α	α	β	2	α
³ Π	0.43	2	2	α	0	β	α	β	2	α
	-0.38	2	2	α	0	2	0	β	2	α
	-0.31	2	2	α	0	β	α	2	β	α
³ Σ ⁻	0.33	2	2	2	0	β	α	β	α	α
	-0.33	2	2	2	0	2	0	β	α	α
	-0.33	2	2	2	0	β	α	2	0	α
	0.33	2	2	2	0	2	0	2	0	α
⁵ Σ ⁻	0.54	2	2	2	0	β	α	α	α	α
⁷ Σ ⁻	1.00	2	2	2	0	α	α	α	α	α
⁵ Σ ⁺	0.74	2	2	0	0	2	α	2	α	α
³ Π	0.63	2	2	α	0	2	β	2	0	α
³ Φ	-0.53	2	2	0	0	2	α	2	0	2
	0.53	2	2	0	0	2	0	2	α	2
³ Σ ⁺	0.39	2	2	0	0	2	α	β	2	α
³ Δ	-0.34	2	2	0	0	2	α	2	β	α
⁵ Φ	0.31	2	α	α	0	α	α	2	α	β
	0.31	2	2	0	0	α	α	2	α	2
	-0.31	2	2	0	0	2	α	α	α	2
⁵ Π	0.32	2	α	α	0	2	α	β	α	2

	-0.31	2	α	α	0	2	α	α	α	β	2
	-0.31	2	2	0	0	2	α	α	α	α	2
	0.31	2	2	0	0	α	α	2	α	2	α
$^3\Sigma^-$	0.28	2	2	0	0	2	2	β	α	α	α
	0.28	2	2	0	0	β	α	2	2	α	α
	-0.27	2	2	0	0	2	0	2	2	α	α
	-0.27	2	2	0	0	2	2	2	0	α	α
$^7\Sigma^+$	0.68	2	α	α	0	2	α	α	2	α	α
	0.68	2	α	α	0	α	2	2	α	α	α
$^5\Delta$	0.33	2	α	α	0	2	α	β	2	α	α
	-0.33	2	α	α	0	2	α	α	2	β	α
	0.33	2	α	α	0	α	2	2	α	β	α
$^7\Pi$	0.70	2	α	α	0	2	α	α	α	α	2
	0.70	2	α	α	0	α	α	2	α	2	α
$^5\Sigma^-$	0.33	2	α	α	0	α	α	2	2	β	α
	0.33	2	α	α	0	2	2	α	α	β	α
$^7\Phi$	0.70	2	α	α	0	2	α	α	α	α	2
	-0.70	2	α	α	0	α	α	2	α	2	α
$^7\Pi$	0.93	2	α	2	0	α	α	2	α	α	α
$^5\Pi$	0.46	2	α	2	0	α	α	2	α	β	α
$^7\Delta$	-0.71	2	α	α	0	2	α	α	2	α	α
	0.71	2	α	α	0	α	2	2	α	α	α
$^7\Sigma^-$	0.71	2	α	α	0	α	α	2	2	α	α
	0.71	2	α	α	0	2	2	α	α	α	α
$^3\Pi$	0.30	2	α	2	0	2	0	2	α	β	α
	0.30	2	2	β	0	2	0	2	α	α	α

Table S5: Dominant electronic configurations for the twenty-seven electronic states of FeO^{2+} at the equilibrium geometry.

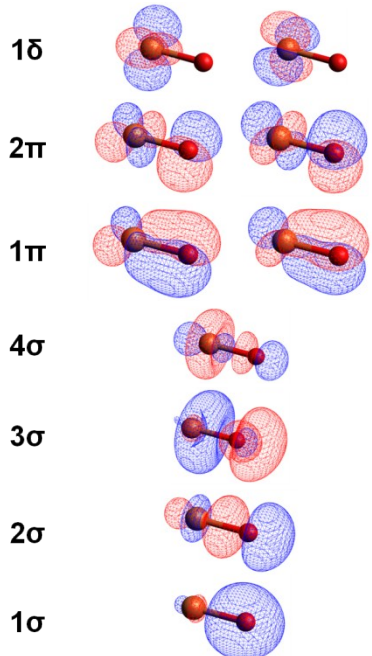


Figure S6: Valence molecular orbitals of ${}^5\Sigma^+$ at its equilibrium bond length.

S4. Analysis the of sigma/pi channels

Potential energy curves of quintet (three) and triplet (six) states are plotted for each model complex. Energy differences are shown with respect to the most stable state (quintet or triplet).

1. $[\text{Fe}(\text{O})(\text{H}_2\text{O})_5]^{2+}$: MS-CASPT2(18,12)

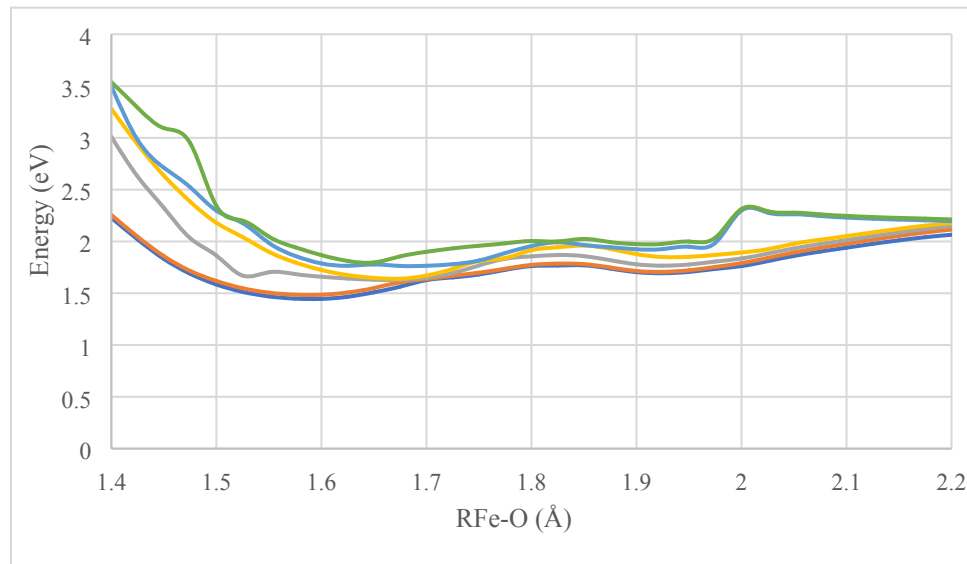


Figure S7: Potential energy curves of $[\text{Fe}(\text{O})(\text{H}_2\text{O})_5]^{2+}$ at the MS-CASPT2(18,12) level for the six lowest triplet states. All energies are shown as differences from the minimum of the quintet ground state.

The second minimum shown in $R_{\text{Fe}-\text{O}} = 1.95 \text{ \AA}$ is due to avoided crossings and issues due to a limited number of multistate CASPT2 calculations with triplet excited states which are less stable at the equilibrium geometry.

Comparison between MS(3)-CASPT2(18,12) and MS(3)-RASPT2(18,12) showed no difference on the three lowest quintet states of $[\text{Fe}(\text{O})(\text{H}_2\text{O})_5]^{2+}$.

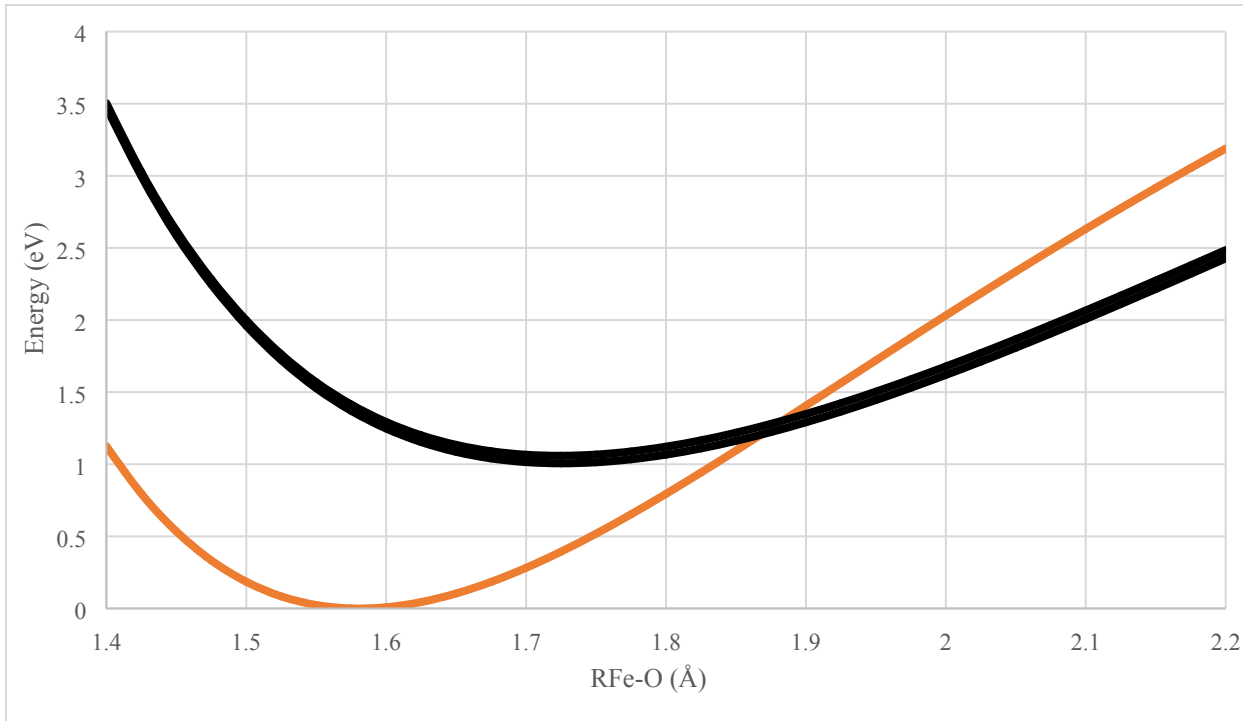


Figure S8: Potential energy curve of $[\text{Fe}(\text{O})(\text{H}_2\text{O})_5]^{2+}$ at the MS(3)-CASPT2(18,12) level.

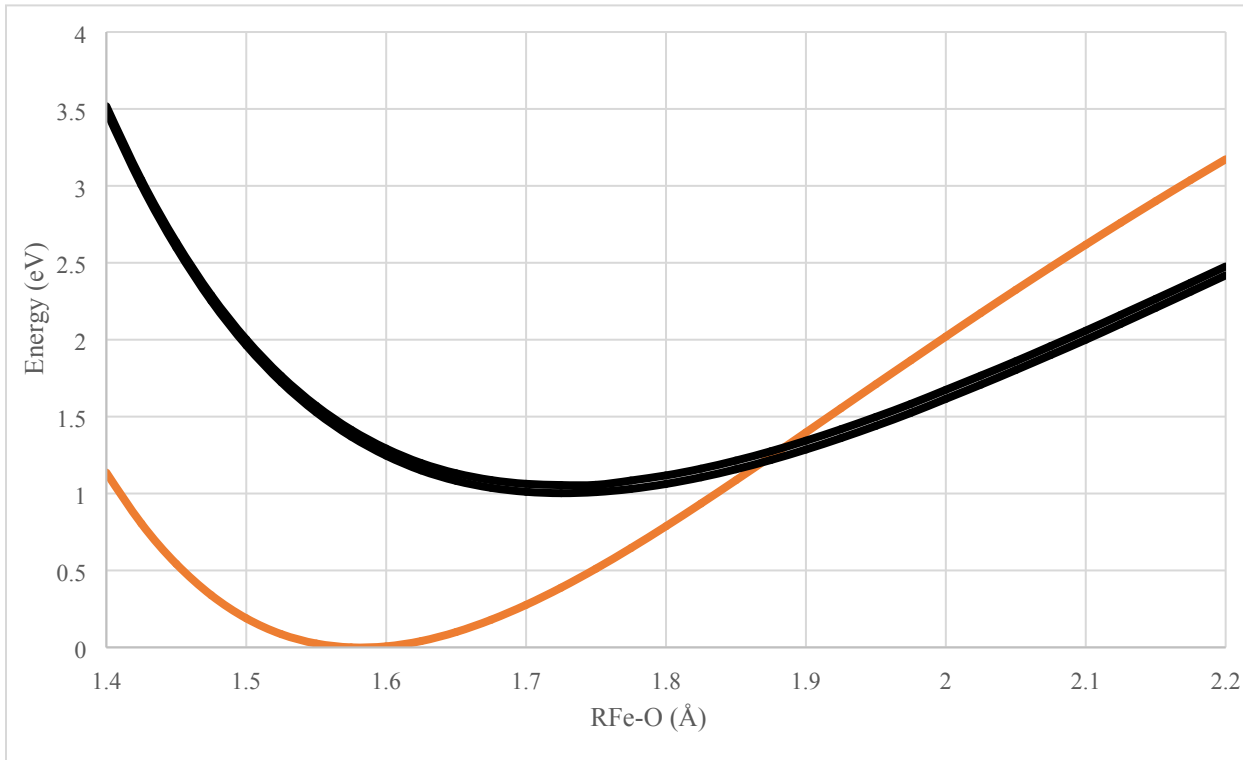


Figure S9: Potential energy curve of $[\text{Fe}(\text{O})(\text{H}_2\text{O})_5]^{2+}$ at the MS(3)-RASPT2(18,12) level.

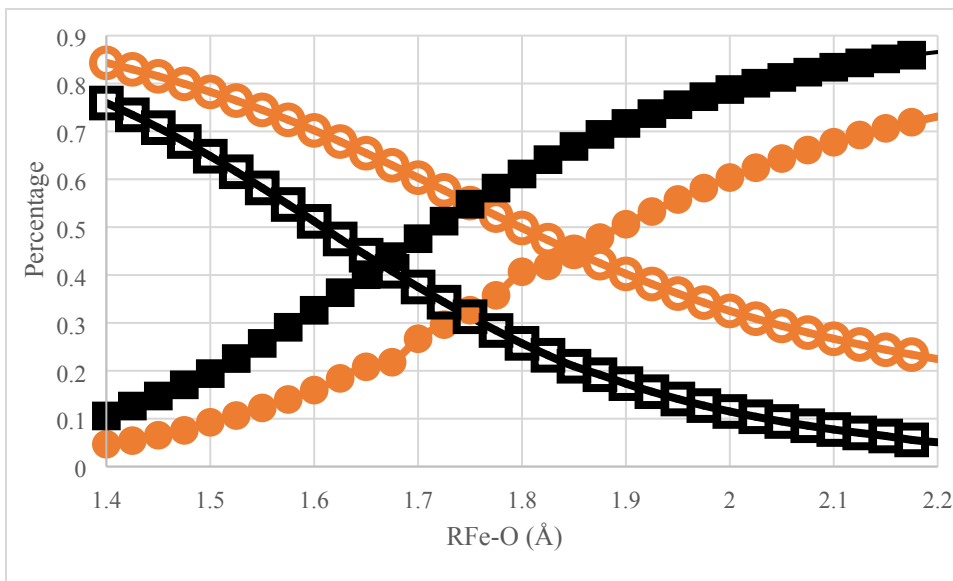
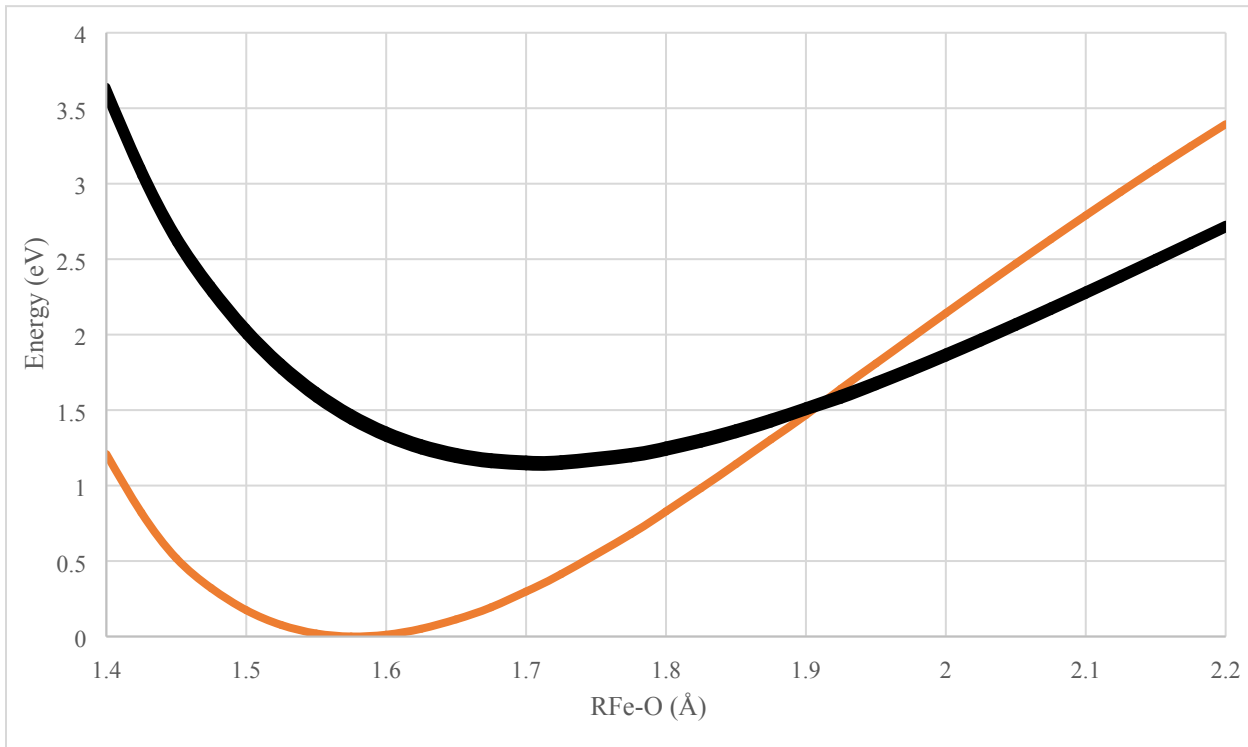


Figure S10: The percentage of the wave function for the ground (${}^5\text{A}$, orange) and first excited state (${}^5\text{E}$, black) of $[\text{Fe}(\text{O})(\text{H}_2\text{O})_5]^{2+}$ along the Fe-O bond distance which corresponds to the non-reactive Fe(IV)-oxo electronic configuration (open circles and squares, respectively) and to the radical Fe(III)-oxyl configuration (closed circles and squares, respectively).

2. $[\text{Fe}(\text{O})(\text{H}_2\text{O})_4]^{2+}$: MS-CASPT2(20,13)

Figure S11: Potential energy curves of $[\text{Fe}(\text{O})(\text{H}_2\text{O})_4]^{2+}$ at the MS-CASPT2(20,13) level for the three lowest quintet states.



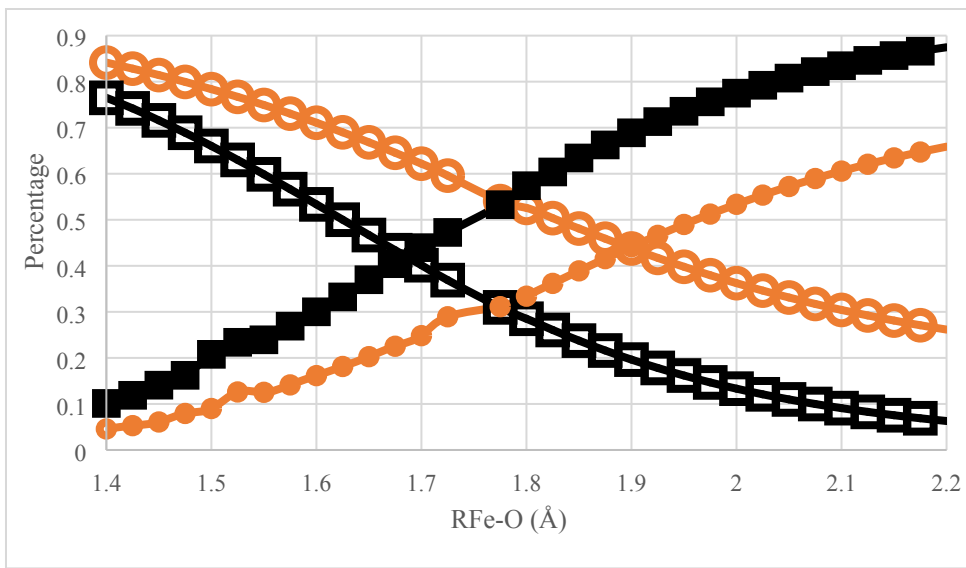


Figure S12: The percentage of the wave function for the ground (^5A , orange) and first excited state (^5E , black) of $[\text{Fe}(\text{O})(\text{H}_2\text{O})_4]^{2+}$ along the Fe-O bond distance which corresponds to the non-reactive Fe(IV)-oxo electronic configuration (open circles and squares, respectively) and to the radical Fe(III)-oxyl configuration (closed circles and squares, respectively).

3. $[\text{Fe}(\text{O})(\text{H}_2\text{O})_{\text{ax}}(\text{NH}_3)_3]^{2+}$: MS-CASPT2(20,13)

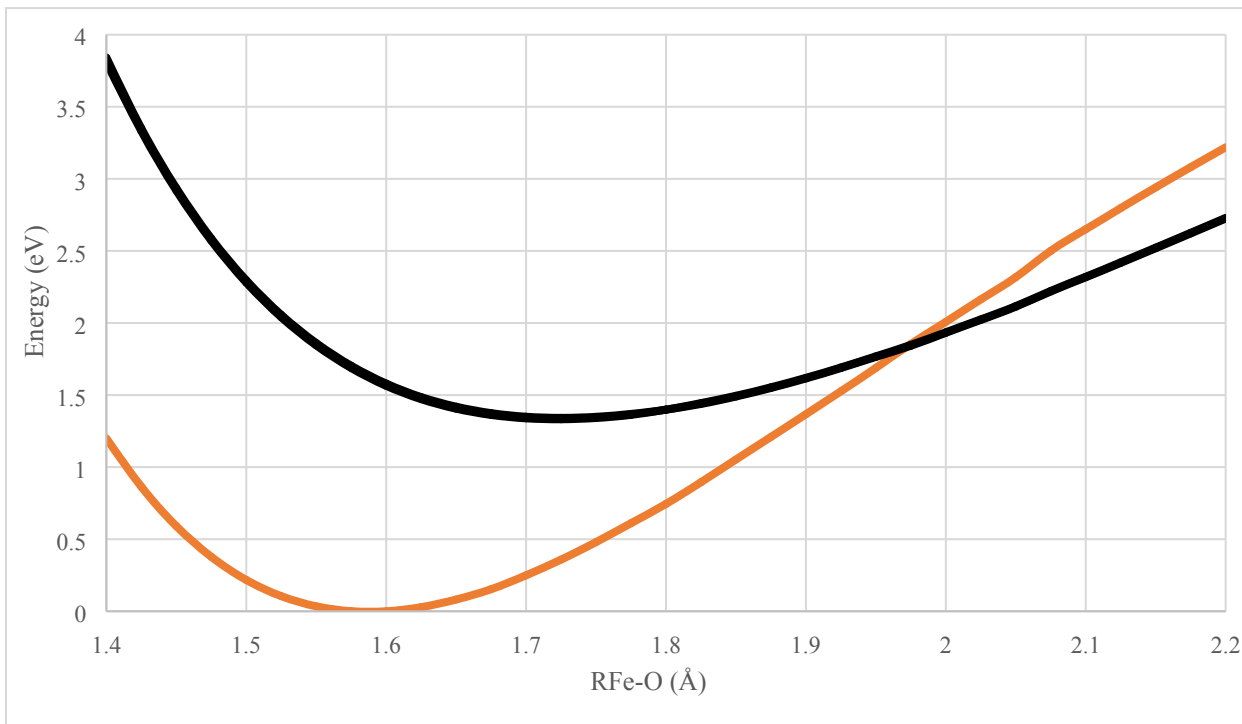


Figure S13: Potential energy curves of $[\text{Fe}(\text{O})(\text{H}_2\text{O})_{\text{ax}}(\text{NH}_3)_3]^{2+}$ at the MS-RASPT2(22,14) level for the three lowest quintet states.

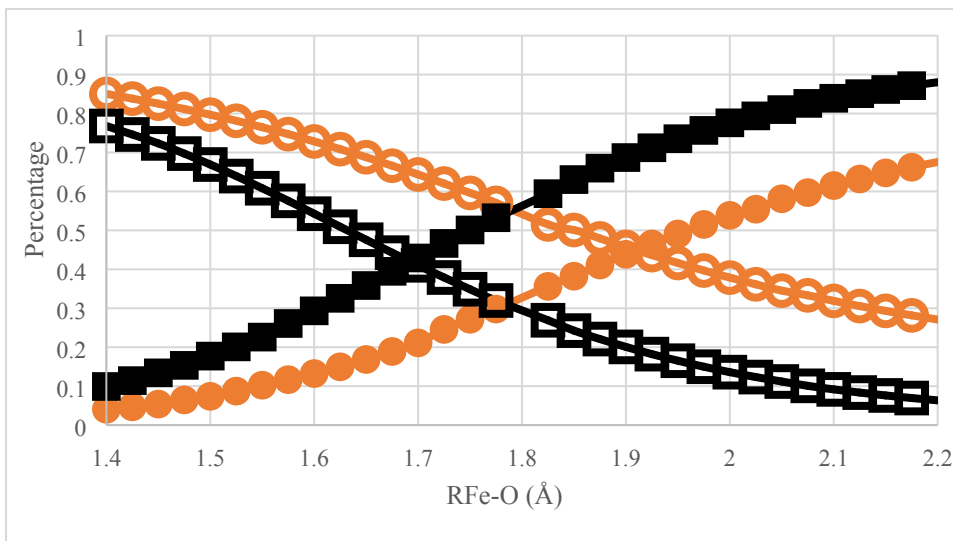


Figure S14: The percentage of the wave function for the ground (5A , orange) and first excited state (5E , black) of $[\text{Fe}(\text{O})(\text{H}_2\text{O})_{\text{ax}}(\text{NH}_3)_3]^{2+}$ along the Fe-O bond distance which corresponds to the non-reactive Fe(IV)-oxo electronic configuration (open circles and squares, respectively) and to the radical Fe(III)-oxyl configuration (closed circles and squares, respectively).

4. $[\text{Fe}(\text{O})(\text{H}_2\text{O})_{\text{ax}}(\text{NH}_3)_4]^{2+}$ MS-CASPT2(18,12)

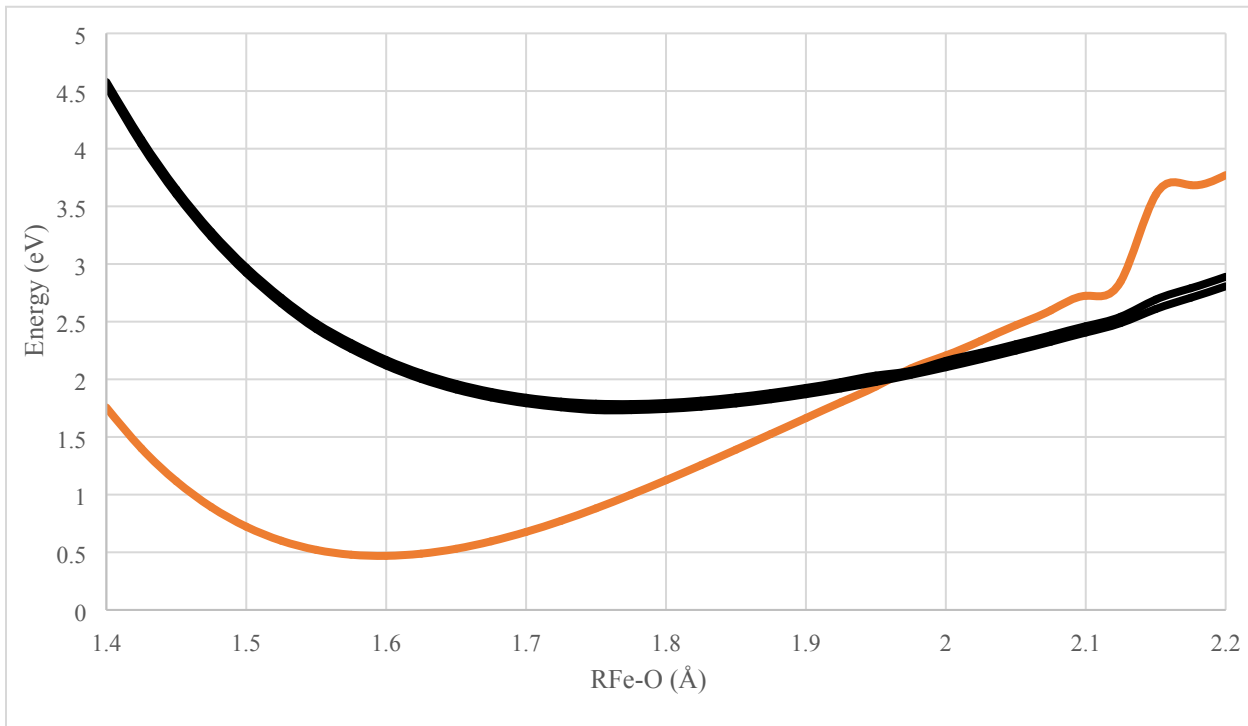


Figure S15: Potential energy curves of $[\text{Fe}(\text{O})(\text{H}_2\text{O})_{\text{ax}}(\text{NH}_3)_4]^{2+}$ at the MS-RASPT2(24,15) level for the three lowest quintet states. All energies are shown as differences from the minimum of the triplet ground state.

The second minimum shown in $R_{\text{Fe}-\text{O}} = 2.15 \text{ \AA}$ is due to avoided crossings and issues due to a limited number of multistate CASPT2 calculations with quintet excited states which are less stable

at the equilibrium geometry. Since the avoided crossings occur beyond the intercrossing of the $^5\text{A}/^5\text{E}$ states, they do not affect the analysis of our results.

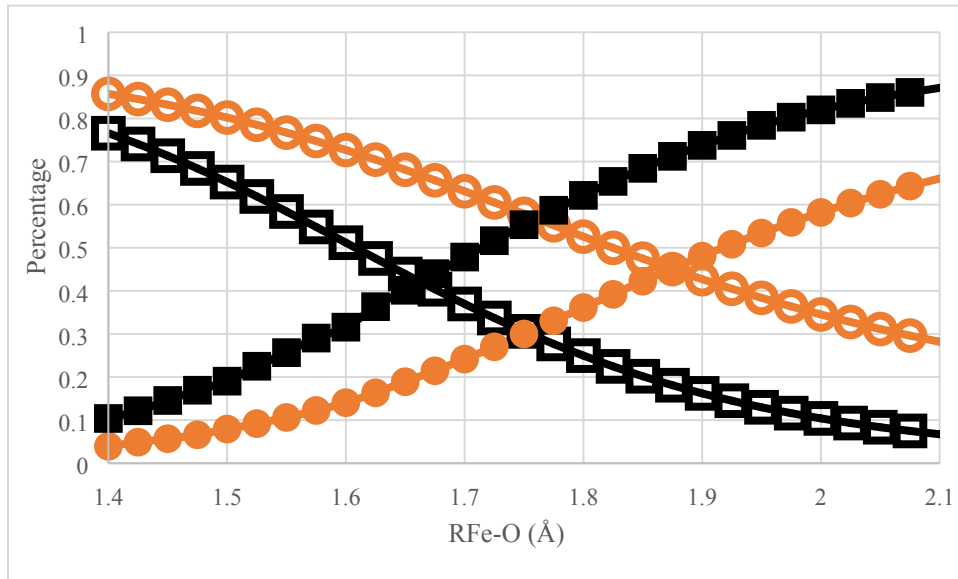


Figure S16: The percentage of the wave function for the ground (^5A , orange) and first excited state (^5E , black) of $[\text{Fe}(\text{O})(\text{H}_2\text{O})_{\text{ax}}(\text{NH}_3)_4]^{2+}$ along the Fe-O bond distance which corresponds to the non-reactive Fe(IV)-oxo electronic configuration (open circles and squares, respectively) and to the radical Fe(III)-oxyl configuration (closed circles and squares, respectively).

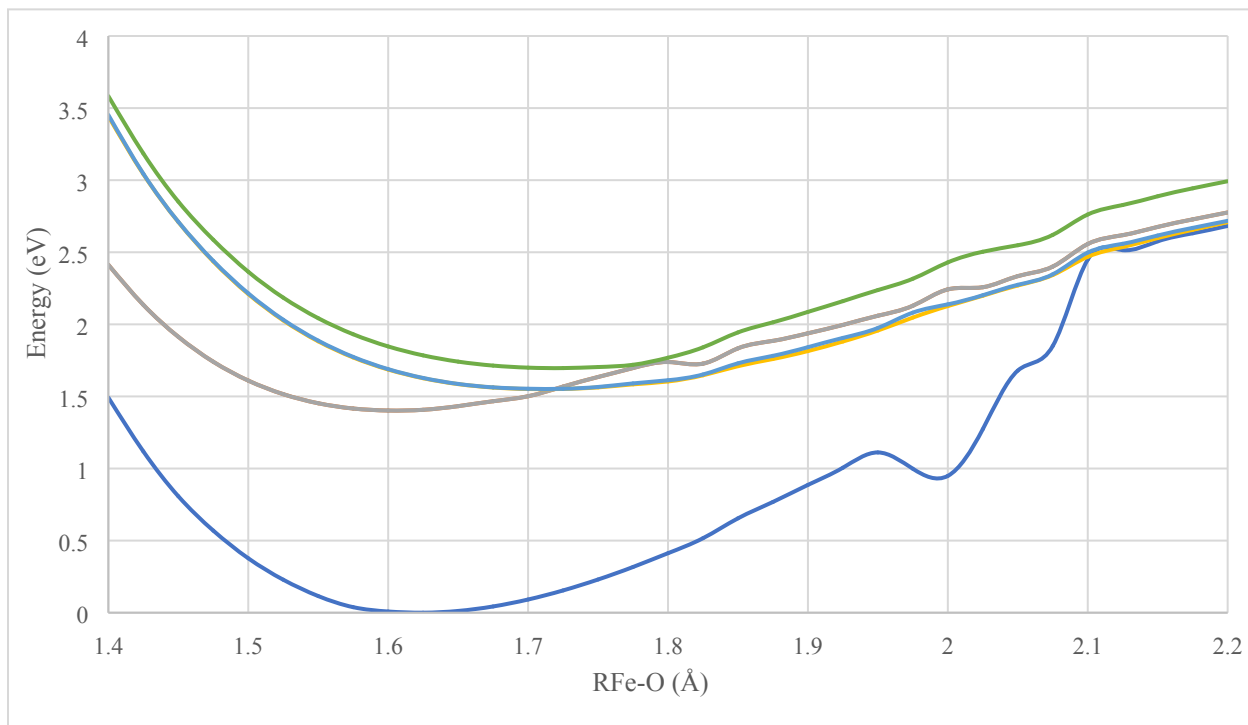


Figure S17: Potential energy curves of $[\text{Fe}(\text{O})(\text{H}_2\text{O})_{\text{ax}}(\text{NH}_3)_3]^{2+}$ at the MS-RASPT2(20,13) level for the six lowest triplet states.

The second minimum shown at $R_{\text{Fe-O}} = 2.00 \text{ \AA}$ is due to avoided crossings and issues due to a limited number of multistate CASPT2 calculations with triplet excited states which are less stable at the equilibrium geometry.

5. $[\text{Fe}(\text{O})(\text{NH}_3)_4]^{2+}$: MS-CASPT2(20,13)

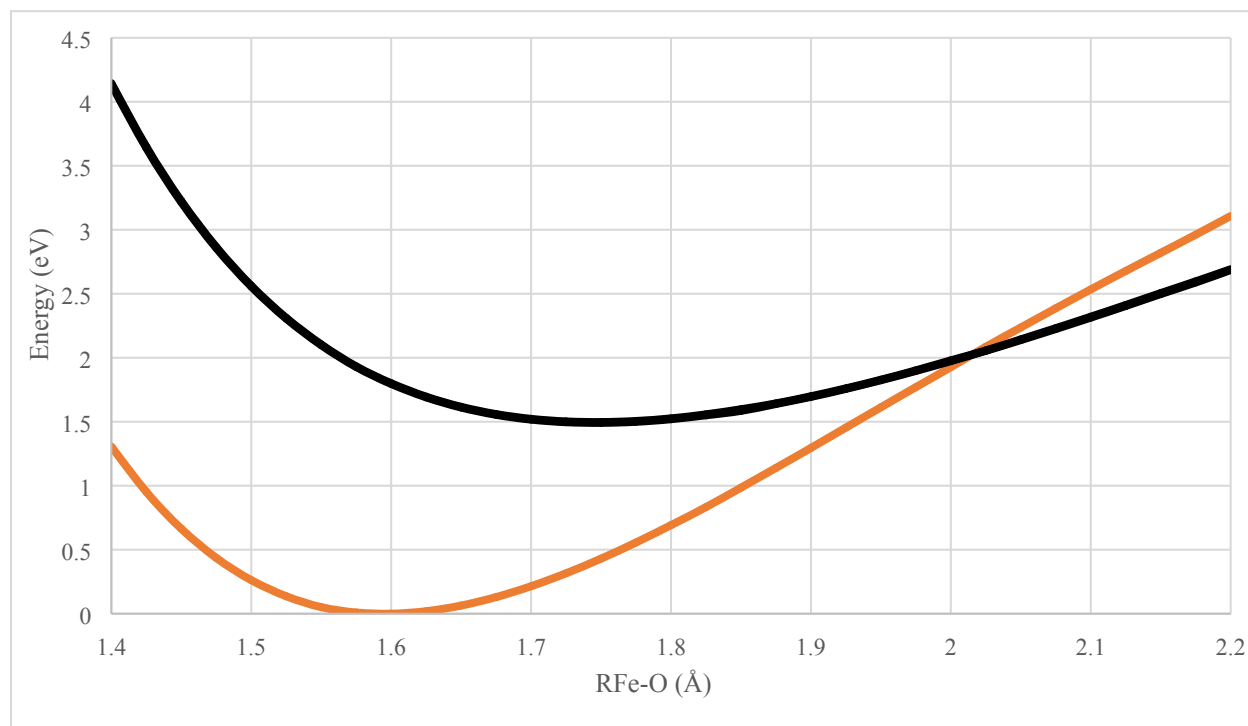


Figure S18: Potential energy curves of $[\text{Fe}(\text{O})(\text{NH}_3)_4]^{2+}$ at the MS-RASPT2(20,13) level for the three lowest quintet states.

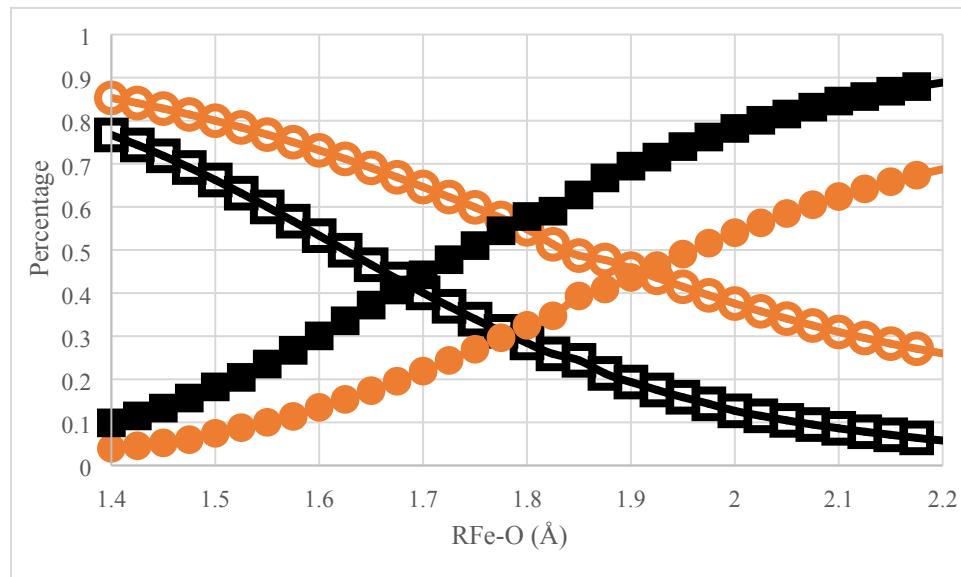


Figure S19: The percentage of the wave function for the ground (^5A , orange) and first excited state (^5E , black) of $[\text{Fe}(\text{O})(\text{NH}_3)_4]^{2+}$ along the Fe-O bond distance which corresponds to the non-reactive Fe(IV)-oxo electronic configuration (open circles and squares, respectively) and to the radical Fe(III)-oxyl configuration (closed circles and squares, respectively).

6. $[\text{Fe}(\text{O})(\text{NH}_3)_5]^{2+}$: MS-CASPT2(18,12)

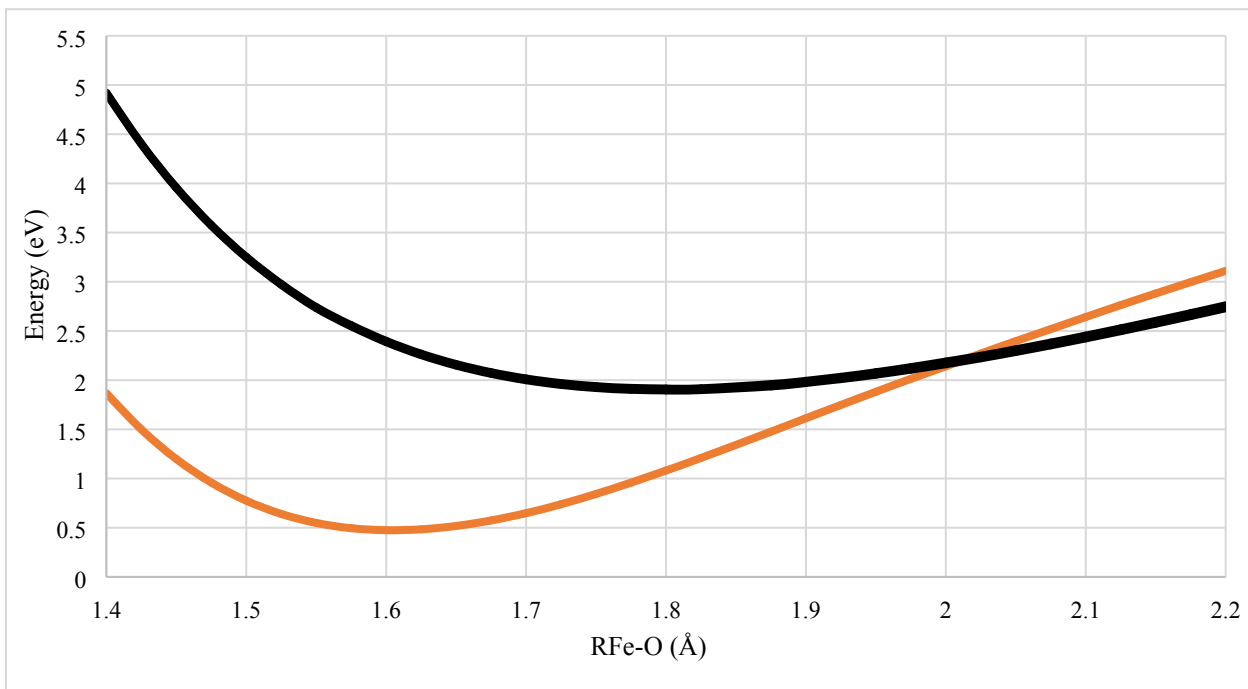


Figure S20. Potential energy curves of $[\text{Fe}(\text{O})(\text{NH}_3)_5]^{2+}$ at the MS-CASPT2(18,12) level for the three lowest quintet states.

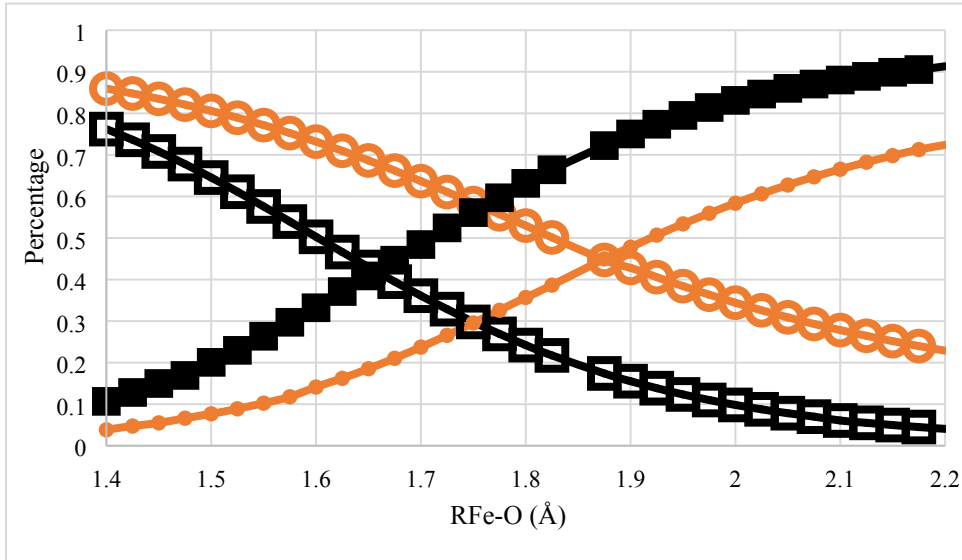


Figure S21. The percentage of the wave function for the ground (^5A , orange) and first excited state (^5E , black) of $[\text{Fe}(\text{O})(\text{NH}_3)_5]^{2+}$ along the Fe-O bond distance which corresponds to the non-reactive Fe(IV)-oxo electronic configuration (open circles and squares, respectively) and to the radical Fe(III)-oxyl configuration (closed circles and squares, respectively).

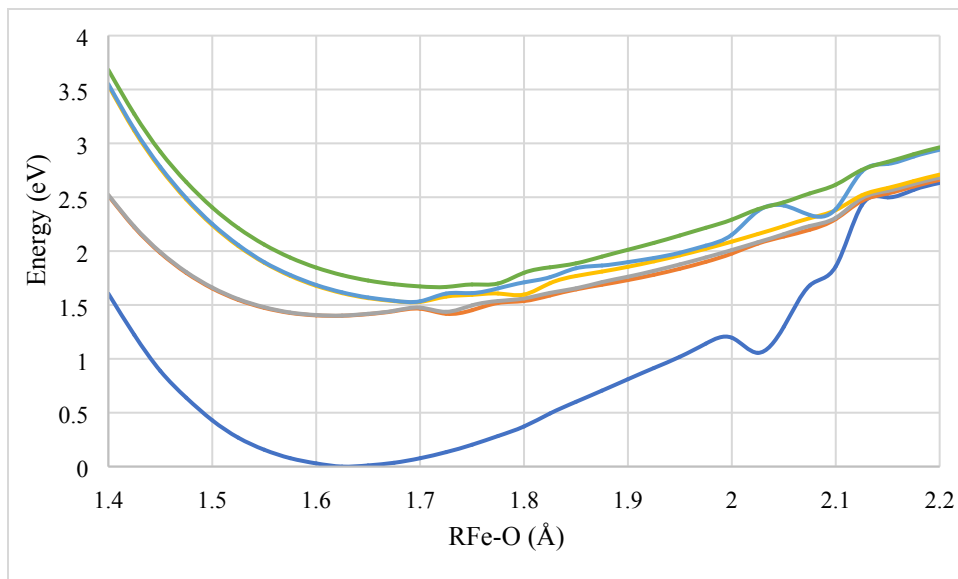


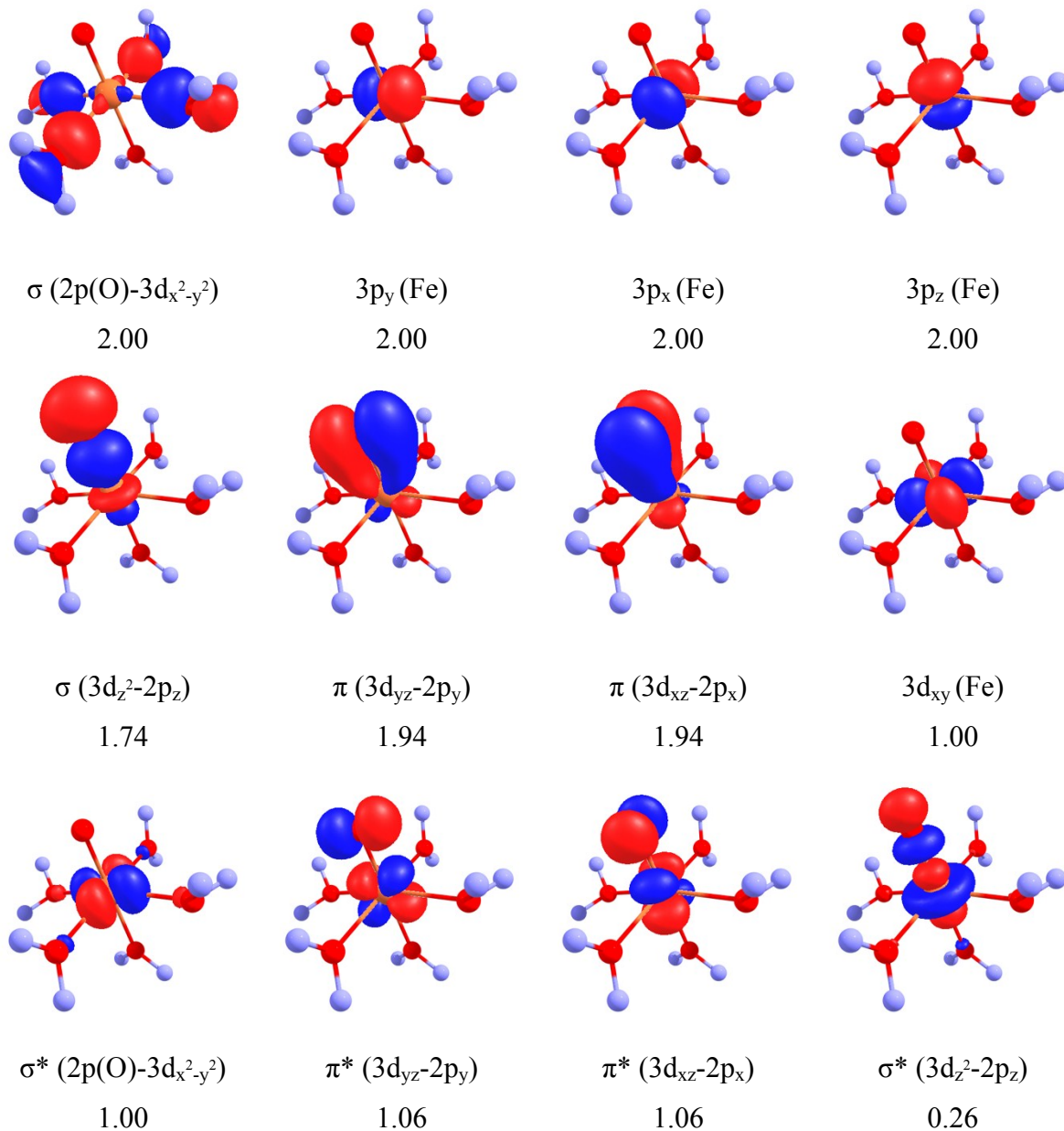
Figure S22: Potential energy curves of $[\text{Fe}(\text{O})(\text{NH}_3)_4]^{2+}$ at the MS-RASPT2(18,12) level for the six lowest triplet states.

S5. CASSCF/RASSCF Active Spaces

Molecular orbital isosurfaces with a contour value of 0.075 a.u.. All orbitals generated at an $R_{\text{Fe-O}}$ of 1.6Å.

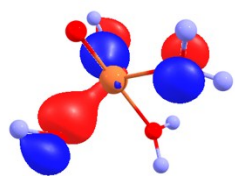
1. $[\text{Fe}(\text{O})(\text{H}_2\text{O})_5]^{2+}$

CAS(18,12)



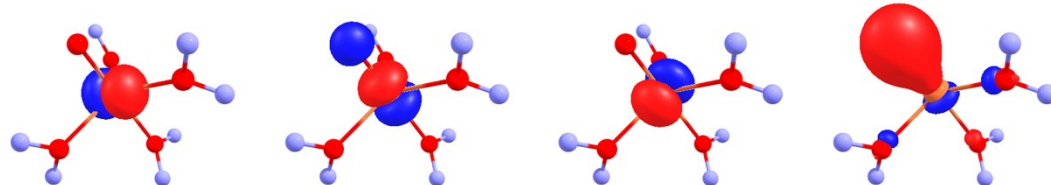
2. $[\text{Fe}(\text{O})(\text{H}_2\text{O})_4]^{2+}$

CAS(20,13)



σ ($2\text{p}(\text{O})$ - $3\text{d}_{x^2-y^2}$)

2.00



3p_x (Fe)

2.00

3p_z (Fe)

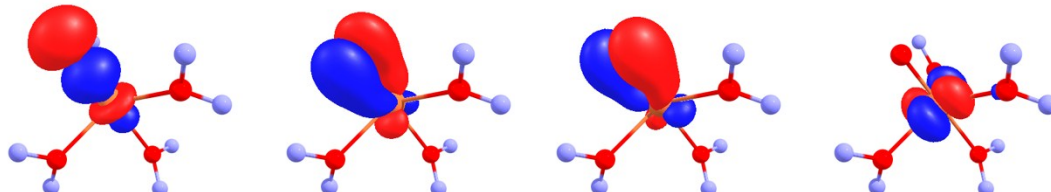
2.00

3p_y (Fe)

2.00

2s (O)

2.00



σ (3d_{z^2} - 2p_z)

1.75

π (3d_{yz} - 2p_y)

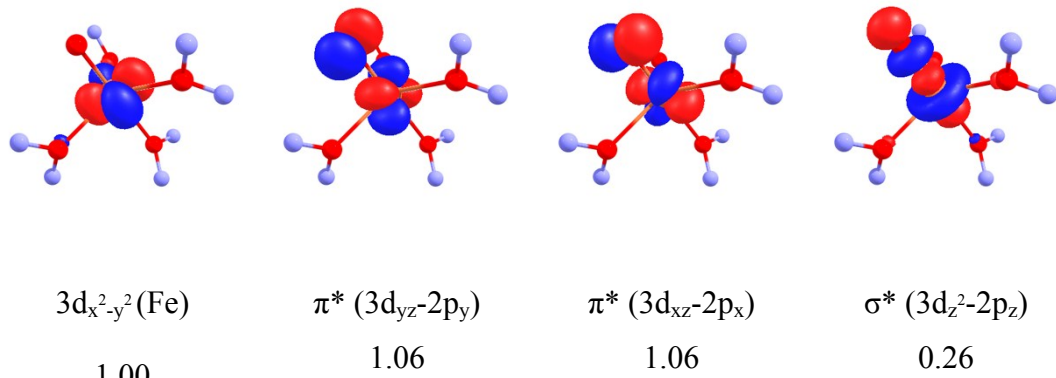
1.94

π (3d_{xz} - 2p_x)

1.94

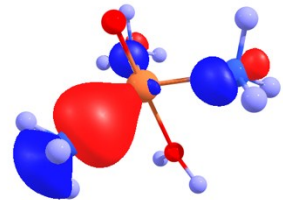
3d_{xy} (Fe)

1.00

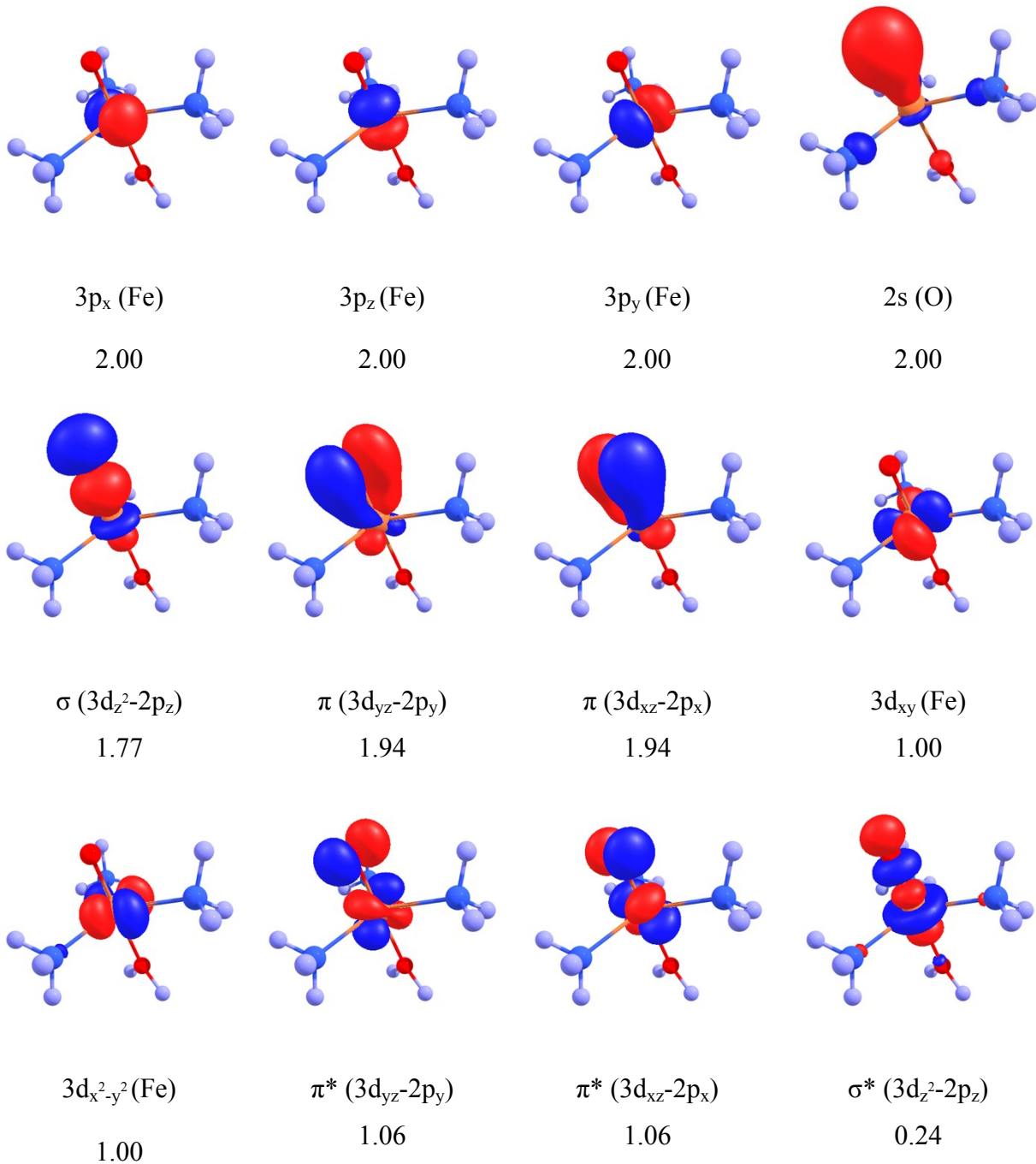


3. $[\text{Fe}(\text{O})(\text{H}_2\text{O})_{\text{ax}}(\text{NH}_3)_3]^{2+}$

CAS(20,13)

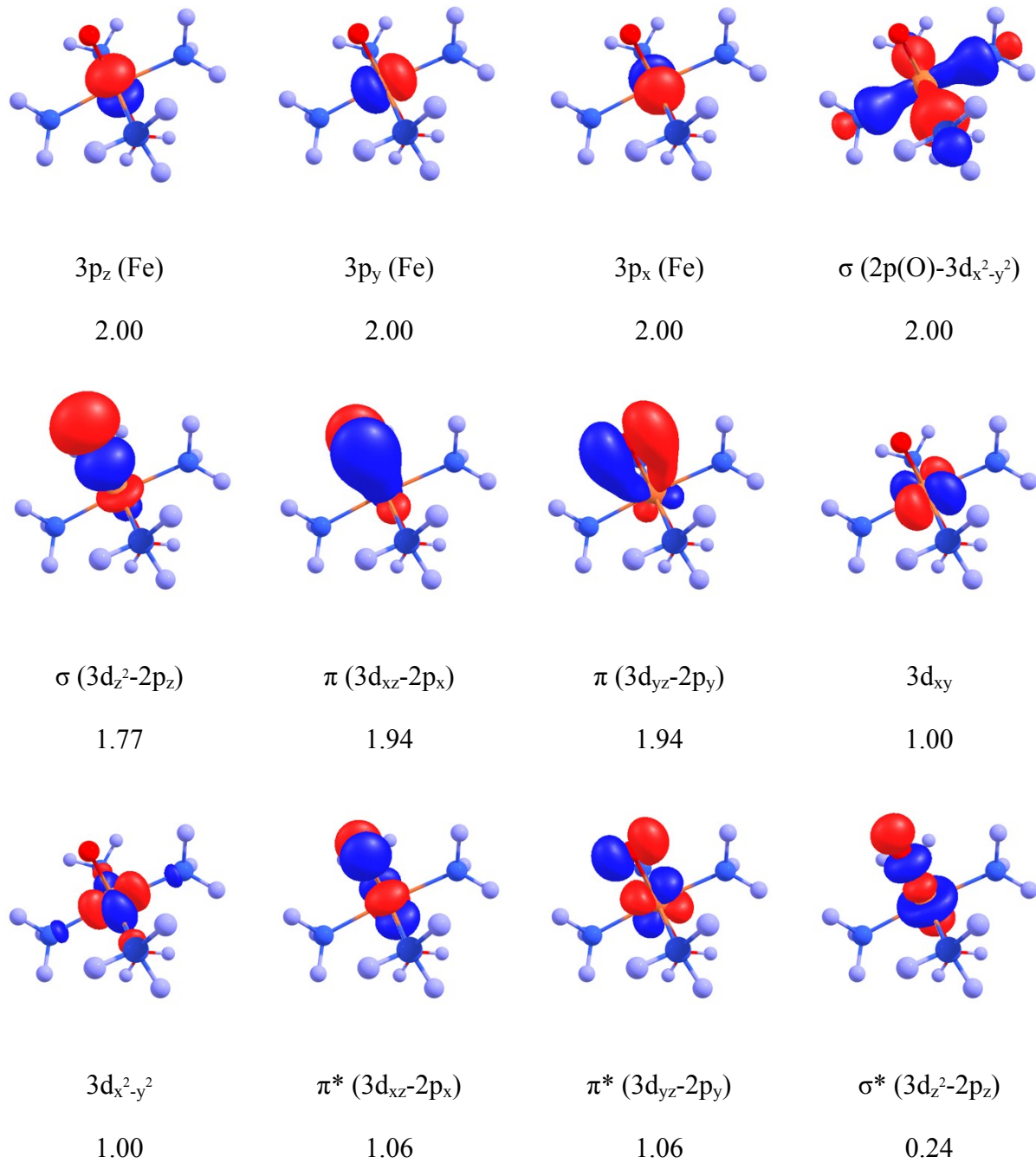


$\sigma(2p(\text{O})-3d_{x^2-y^2})$
 2.00



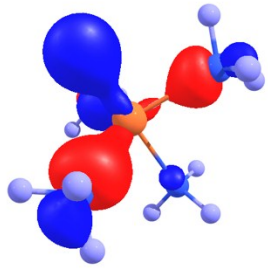
4. $[\text{Fe}(\text{O})(\text{H}_2\text{O})_{\text{ax}}(\text{NH}_3)_4]^{2+}$

CAS(18,12)



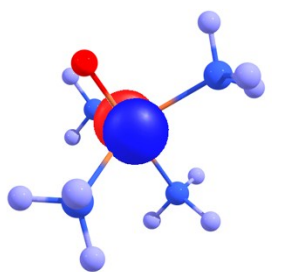
5. [Fe(O)(NH₃)₄]²⁺

CAS(20,13)



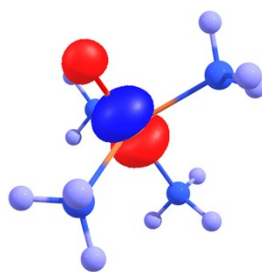
σ ($2p(O)$ - $3d_{x^2-y^2}$)

2.00



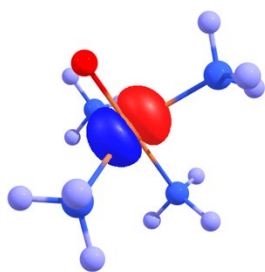
$3p_x$ (Fe)

2.00



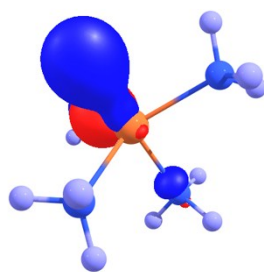
$3p_z$ (Fe)

2.00



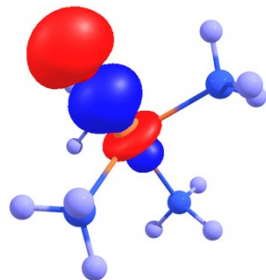
$3p_y$ (Fe)

2.00



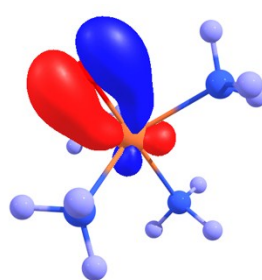
$2s$ (O)

2.00



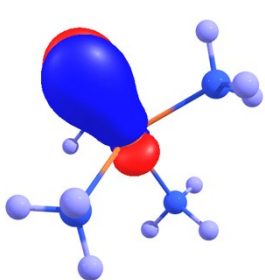
σ ($3d_z^2$ - $2p_z$)

1.78



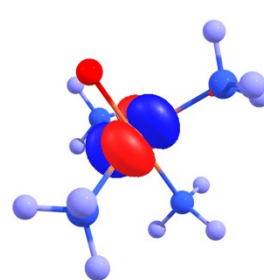
π ($3d_{yz}$ - $2p_y$)

1.93



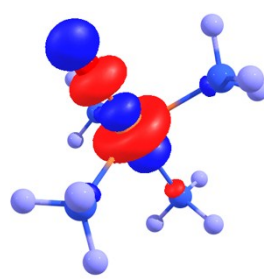
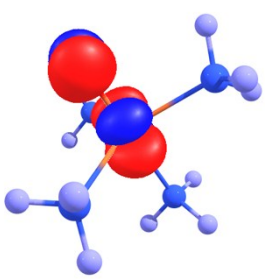
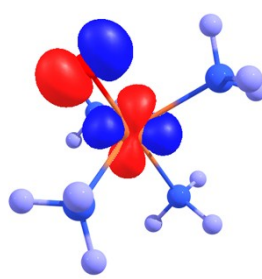
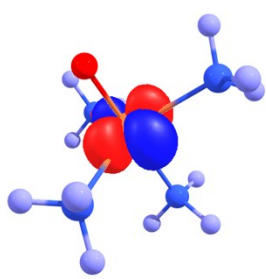
π ($3d_{xz}$ - $2p_x$)

1.93



$3d_{xy}$ (Fe)

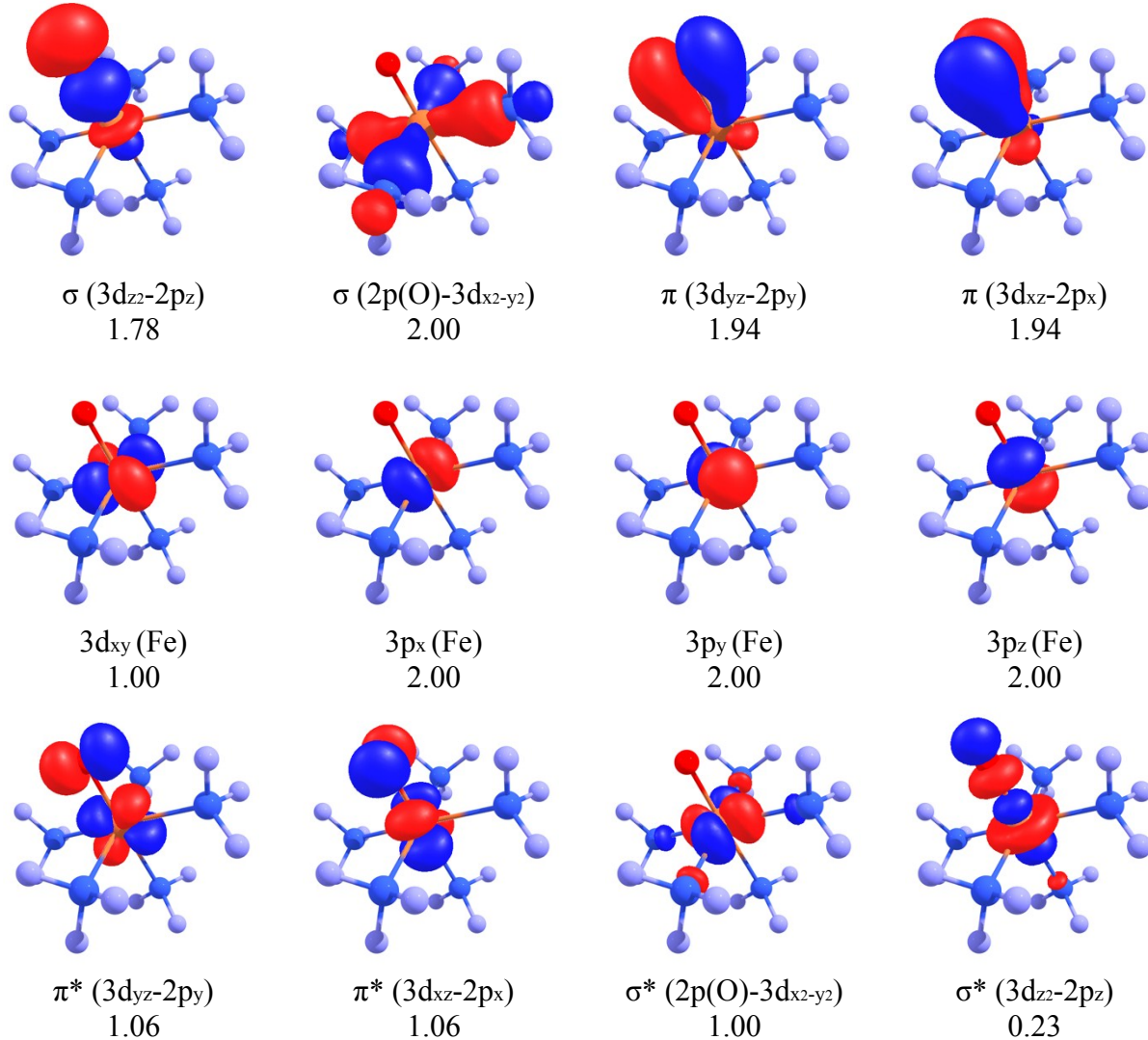
1.00



$3d_{x^2-y^2}(Fe)$	$\pi^*(3d_{yz}-2p_y)$	$\pi^*(3d_{xz}-2p_x)$	$\sigma^*(3d_{z^2}-2p_z)$
1.00	1.07	1.07	0.23

6. $[Fe(O)(NH_3)_5]^{2+}$

CAS(18,12)



S6. Geometry Coordinates from Symmetric Ligand Scan Geometries

Color coding: Red = Oxygen, Pink = Iron, Blue = Hydrogen, Nitrogen = Purple

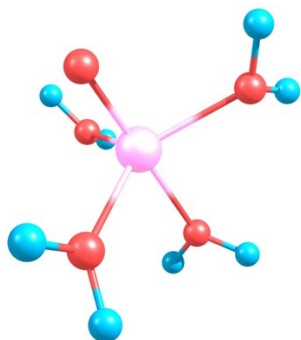
- $[\text{FeO}(\text{NH}_3)]^{2+}$

Fe	-0.4043506589	0.0000000000	-0.2070793284
O	0.9613167155	0.0000000000	-1.0687414421
N	0.3926021986	0.0000000000	1.6192168835
H	-0.2942447731	0.0000000000	2.3735054713
H	0.9915274968	0.8100677496	1.7817255274
H	0.9915274968	-0.8100677496	1.7817255274

- $[\text{FeO}(\text{H}_2\text{O})]^{2+}$

Fe	0.0000000000	0.4017531482	-0.1881917559
O	0.0000000000	-0.9089368885	-1.1379030084
O	0.0000000000	-0.4097203036	1.5365100107
H	0.0000000000	-1.3652975570	1.7021000376
H	0.0000000000	0.0368611554	2.3978187245

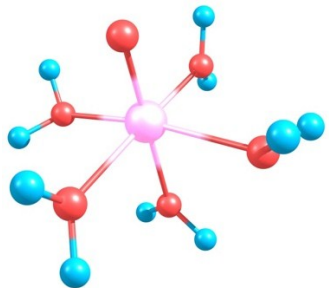
- $[\text{Fe}(\text{O})(\text{H}_2\text{O})_4]^{2+}$



O	1.974997387	0.000000000	-0.003212361
O	-0.971915766	-1.718838285	-0.039996173
O	-1.039779114	1.678614122	-0.041701598

O	0.002259902	-0.000462147	-2.097228345
O	0.000000000	0.000000000	1.600000000
H	2.600549515	0.138256617	-0.737645072
H	2.484537632	0.032077690	0.829222289
H	-1.598335225	-2.049065927	-0.711029593
H	-1.205098860	-2.158707585	0.800745280
H	-1.727498747	1.943153927	-0.681634000
H	-1.275043808	2.105323428	0.805604936
H	0.210403233	-0.763346794	-2.666962796
H	0.085269318	0.777762267	-2.677872367
Fe	0.000000000	0.000000000	0.000000000

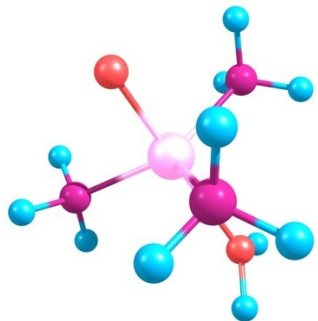
- [Fe(O)(H₂O)₅]²⁺



O	-0.025324230	-2.049417997	-0.041767885
O	0.018849756	2.049408663	-0.045484229
O	-2.091357365	-0.003399065	-0.190296653
O	2.091724903	0.000000000	-0.186244274
O	0.000000000	0.000000000	-2.050000000

O	0.000000000	0.000000000	1.600000000
H	0.260399742	-2.632099615	-0.767385167
H	0.049613005	-2.570390225	0.778375753
H	-0.256547139	2.632281806	-0.774863295
H	-0.050403127	2.574707980	0.772321401
H	-2.580231187	0.463152843	0.513968066
H	-2.524603255	-0.876801455	-0.228070598
H	2.527469540	0.870553159	-0.250799077
H	2.578388690	-0.445707735	0.532921650
H	-0.775217582	0.084068720	-2.630623087
H	0.770013452	-0.102120708	-2.634583142
Fe	0.000000000	0.000000000	0.000000000

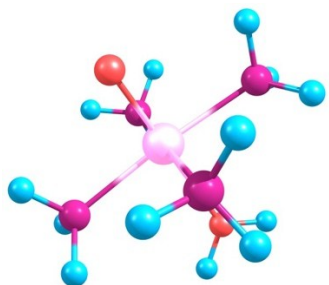
- $[\text{Fe}(\text{O})(\text{H}_2\text{O})_{\text{ax}}(\text{NH}_3)_3]^{2+}$



H	-1.969017521	1.763896885	-0.179520430
N	2.049920395	0.000000000	0.018065784
H	2.378612673	0.463383954	0.875685970
H	2.460258679	-0.943262945	0.060926736

N	-1.063186751	-1.752357423	0.037113271
H	-0.547796050	-2.483872511	0.545826459
H	-1.932139033	-1.636509780	0.576587934
H	2.519998137	0.476816421	-0.762537668
H	-0.878691937	2.233643157	0.939027862
H	-1.334910020	-2.163671736	-0.864510777
O	0.000000000	0.000000000	1.600000000
O	0.023772286	0.034298795	-2.130703119
H	0.592206090	-0.498664922	-2.713403512
H	-0.671387869	0.376299128	-2.719225917
Fe	0.000000000	0.000000000	0.000000000
N	-0.957193918	1.812805740	0.003892893
H	-0.588802491	2.513246081	-0.653550623

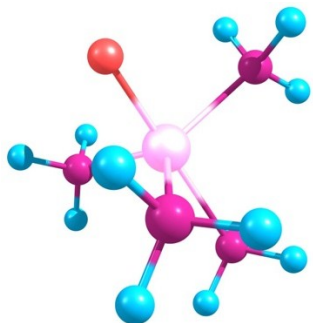
- [Fe(O)(H₂O)_{ax}(NH₃)₄]²⁺



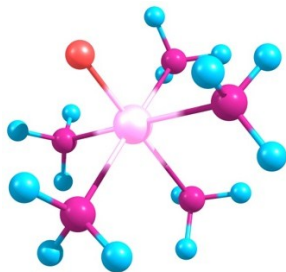
N	0.011818146	1.997840616	-0.092158574
N	-0.016060516	-1.997953654	-0.089012677
N	1.999986438	0.000000000	0.007365269

N	-1.999964367	0.011728931	0.002227813
O	0.000000000	0.000000000	1.575000000
H	0.848903420	2.443380110	-0.486656209
H	-0.034601525	2.346750995	0.873429167
H	0.772723204	-2.463294938	-0.553839200
H	0.010070559	-2.345791853	0.877704124
H	2.360876469	0.745711942	0.614344185
H	2.383678888	-0.855526283	0.426177414
Fe	0.000000000	0.000000000	0.000000000
H	2.483454428	0.108160151	-0.891741174
H	-0.847283168	-2.439346777	-0.500311887
H	-2.375801146	-0.755880160	0.571519557
H	-2.380296956	0.852313979	0.452992615
H	-0.769838111	2.458729566	-0.573197146
H	-2.470153867	-0.053712237	-0.908000542
O	-0.021256122	-0.005841773	-2.174543858
H	0.057494079	-0.772889174	-2.763736134
H	-0.001455858	0.761695292	-2.768040971

- [Fe(O)(NH₃)₄]²⁺



Fe	0.000000000	0.000000000	0.000000000
N	-0.996851010	-1.762200247	0.039539291
H	-1.897983673	-1.785930465	-0.455955936
H	-0.470214318	-2.571280305	-0.316399273
N	0.000003427	-0.000010763	-2.143701232
H	-0.932774168	-0.026540562	-2.576390633
H	0.446424488	0.822271644	-2.571343279
N	-1.017361522	1.749689804	0.064700249
H	-1.656506274	1.731826218	0.870660883
H	-0.390135460	2.542808792	0.257718112
N	2.023654895	0.000000000	0.073796110
H	2.349470234	0.785404903	0.653570964
H	2.354062100	-0.832197699	0.581415294
H	-1.584211402	2.036992641	-0.742795344
H	-1.213918609	-1.989454686	1.018509857
H	2.575763671	0.040020046	-0.791608476
H	0.489549476	-0.797329650	-2.571199188
O	0.000000000	0.000000000	1.625000000



N -2.0684900 0.2405462 -0.0378584
N 2.0387532 -0.2337470 -0.1740065
N -0.2827677 -2.0453708 -0.1475585
N 0.1893428 2.0632335 -0.1330840
N 0.0930517 -0.0151201 2.0698087
O -0.0637871 0.0157128 -1.7449848
H -2.5846588 -0.5139995 0.4132369
H -2.3964865 0.2712763 -1.0039742
H 2.4009582 -1.0811794 0.2614763
H 2.2978936 -0.2834534 -1.1602483
H -0.8435991 -2.2616141 -0.9720916
H 0.5801311 -2.5719806 -0.2780429
H 0.5160100 -0.8620062 2.4493929
H 0.6508541 0.7458829 2.4570273
Fe -0.0149291 0.0049672 -0.1292325
H -0.7527503 -2.4714422 0.6506252
H 2.5860913 0.5268184 0.2269483
H -0.8089068 0.0583244 2.5401588

H 1.1520692 2.3863830 -0.2206220

H -0.2744240 2.3996800 -0.9774833

H -2.3991583 1.0996054 0.4003135

H -0.2082999 2.5811348 0.6499211

References

- (1) Kazaryan, A.; Baerends, E. J., Ligand Field Effects and the High Spin–High Reactivity Correlation in the H Abstraction by Non-Heme Iron(IV)–Oxo Complexes: A DFT Frontier Orbital Perspective. *ACS Catal.* **2015**, *5*, 1475–1488.
- (2) Andrikopoulos, P. C.; Michel, C.; Chouzier, S.; Sautet, P., In Silico Screening of Iron-Oxo Catalysts for CH Bond Cleavage. *ACS Catal.* **2015**, *5*, 2490–2499.
- (3) Manni, G. L.; Smart, S. D.; Alavi, A., Combining the Complete Active Space Self-Consistent Field Method and the Full Configuration Interaction Quantum Monte Carlo within a Super-Cl Framework, with Application to Challenging Metal-Porphyrins. *J. Chem. Theory Comput.* **2016**, *12*, 1245–1258.
- (4) Radoń, M.; Pierloot, K., Binding of CO, NO, and O₂ to Heme by Density Functional and Multireference ab Initio Calculations. *J. Phys. Chem. A* **2008**, *112*, 11824–11832.
- (5) England, J.; Marlène Martinho; Farquhar, E. R.; Frisch, J. R.; Bominaar, E. L.; Münck, E.; Que, L., A Synthetic High-Spin Oxoiron(IV) Complex: Generation, Spectroscopic Characterization, and Reactivity. *Angew. Chem. Int. Ed.* **2009**, *48*, 3622–3626.
- (6) Lee, C.; Yang, W.; Parr, R. G., Development of the Colle-Salvetti Correlation-Energy Formula into a Functional of the Electron Density. *Phys. Rev. B* **1988**, *37*, 785.
- (7) Becke, A. D., Density-Functional Exchange-Energy Approximation with Correct Asymptotic Behavior. *Phys. Rev. A* **1988**, *38*, 3098.
- (8) Weigend, F.; Ahlrichs, R., Balanced basis sets of split valence, triple zeta valence and quadruple zeta valence quality for H to Rn: Design and assessment of accuracy. *Phys. Chem. Chem. Phys.* **2005**, *7*, 3297–3305.
- (9) Weigend, F., Accurate Coulomb-fitting basis sets for H to Rn. *Phys. Chem. Chem. Phys.* **2006**, *8*, 1057–1065.